2

NASA TECHNICAL NOTE

NASA TN D-7369

NASA TN D-7369

DRAG CHARACTERISTICS OF CIRCULAR CYLINDERS IN A LAMINAR BOUNDARY LAYER AT SUPERSONIC FREE-STREAM VELOCITIES

by Robert L. Stallings, Jr., Milton Lamb, and Dorothy T. Howell

Langley Research Center
Hampton, Va. 23665

NATIONAL AERONAUTICS AND SPACE ADMINISTRATION • WASHINGTON, D. C. • DECEMBER 1973

1. Report No. NASA TN D-7369	2. Government Accession No.	3. Recipient's Catalog No.
4. Title and Subtitle DRAG CHARACTERISTICS OF CIRCULAR CYLINDERS IN A LAMINAR BOUNDARY LAYER AT SUPERSONIC FREE-STREAM VELOCITIES		5. Report Date December 1973 6. Performing Organization Code
7. Author(s) Robert L. Stallings, Jr., Milton Lamb, and Dorothy T. Howell		8. Performing Organization Report No. L-9021 10. Work Unit No. 501-06-05-05
9. Performing Organization Name and Address NASA Langley Research Center Hampton, Va. 23665		11. Contract or Grant No. 13. Type of Report and Period Covered Technical Note
12. Sponsoring Agency Name and Address National Aeronautics and Space Administration Washington, D.C. 20546		14. Sponsoring Agency Code

15. Supplementary Notes

16. Abstract

Drag measurements were obtained with circular cylinders attached to a flat-plate surface with their longitudinal axes perpendicular to the plate surface. When more than one cylinder was tested, they were alined in a spanwise row perpendicular to the free-stream velocity vector. The drag measurements were obtained through a range of Mach numbers from 2.3 to 4.6, cylinder heights ranging from approximately 0.4 to 3 times the undisturbed laminar boundary-layer thickness and cylinder height-to-diameter ratios of 1.0 and approximately 2.

Included in the paper is a complete presentation in figure form of the experimental results and a discussion of the more significant findings. An attempt is made to select the most appropriate parameters for correlating the experimental results and, where possible, these results are compared with theoretical calculations.

17. Key Words (Suggested by Author(s))	18. Distribution Statement		
Cylinder drag Protuberance drag Tripping elements	Unclassified – Unlimited		
19. Security Classif. (of this report) Unclassified	20. Security Classif. (of this page) Unclassified	21. No. of Pages ~~45~~ 46	22. Price* Domestic, $3.00 Foreign, $5.50

*For sale by the National Technical Information Service, Springfield, Virginia 22151

DRAG CHARACTERISTICS OF CIRCULAR CYLINDERS IN A LAMINAR BOUNDARY LAYER AT SUPERSONIC FREE-STREAM VELOCITIES

By Robert L. Stallings, Jr., Milton Lamb, and Dorothy T. Howell
Langley Research Center

SUMMARY

An experimental investigation has been conducted to determine the drag characteristics of circular cylinders attached to a flat-plate surface with their longitudinal axes of symmetry perpendicular to the plate surface. The undisturbed flat-plate boundary layer was laminar at the cylinder installation locations through the range of free-stream variables. The cylinders were alined in a row that was perpendicular to the free-stream velocity vector. Spacing between cylinders was varied from a minimum value of approximately 3 cylinder diameters to an upper-limit value corresponding to an isolated-cylinder installation.

The isolated-cylinder drag coefficient when plotted as a function of the ratio of cylinder height to boundary-layer displacement thickness k/δ^* was found to be invariant with free-stream Mach number and cylinder scale. The magnitude of these experimental values for a cylinder having a height-to-diameter ratio of approximately 2 was in good agreement with results from an approximate theoretical calculation based on a hypothetical cylinder pressure distribution described in the text.

For the row of cylinders, decreasing spacing between cylinders resulted in a reduction in the cylinder drag coefficients. For both the row of cylinders and the isolated cylinders, increasing k/δ^* resulted in an increase in cylinder drag coefficients. If the cylinder drag coefficients for the row of cylinders were normalized by values from the isolated cylinders, however, this normalized parameter was found to be essentially invariant with k/δ^* for $k/\delta^* \gtrsim 2$.

Results obtained from impact-pressure survey through the undisturbed laminar boundary layer on the center line of the flat-plate surface were in good agreement with the theory of NASA TR R-368.

INTRODUCTION

The use of artificial roughness for establishing turbulent boundary layers on wind-tunnel models has been an accepted practice by aerodynamicists for many years. This practice has been applied to flows ranging from incompressible to hypersonic speeds. In

general, increasing tunnel speed results in an increase in the size of roughness required to trip the boundary layer effectively; for example, at subsonic speeds roughness heights only a fraction of the boundary-layer thickness are required (ref. 1), whereas at hypersonic speed roughness heights several times the boundary-layer thickness are required (refs. 2 and 3).

Numerous investigations have also been conducted to define an optimum roughness size and shape for effective boundary-layer tripping, that is, the smallest roughness shape that will move transition to the desired location. Results presented in references 3 and 4 indicate that a circular cylinder, with its longitudinal axis of symmetry perpendicular to the test surface, is an effective tripping element and also the element for which wave drag can be most readily defined. The results of references 3 and 4 were limited to the hypersonic-speed region.

The purpose of the present investigation is to determine the drag of circular cylinders partially or totally submerged in a laminar boundary layer through the higher supersonic-speed region. Results from this investigation can be applied not only to roughness drag on wind-tunnel models but also to cylindrical protuberances in a laminar boundary layer on flight vehicles.

SYMBOLS

A	frontal area of cylinder
C_D	drag coefficient
$C_{D_{IC}}$	drag coefficient of isolated cylinder
C_p	pressure coefficient, $\frac{p - p_\infty}{q_\infty}$
$C_{p,b}$	base pressure coefficient
c_f	local skin-friction coefficient
k	cylinder height
M	Mach number
p	static pressure

$p_{t,2}$ pitot pressure

q dynamic pressure

R Reynolds number based on free-stream conditions and distance from plate leading edge to cylinder installation location

r cylinder radius

S surface area

s spacing between cylinders

u local velocity component parallel to flat-plate model center line

V_∞ free-stream velocity

w cylinder diameter

x, y, θ model coordinates (see sketch A1)

y_{cp} value of y at center-of-pressure location on cylinder

δ boundary-layer thickness

δ^* boundary-layer displacement thickness

γ ratio of specific heats (1.4 for air)

Subscripts:

ℓ local conditions at outer edge of boundary layer

SL at stagnation line of cylinder

∞ free stream

TEST FACILITY

This investigation was conducted in the high Mach number test section of the Langley Unitary Plan wind tunnel, which is a variable-pressure continuous-flow facility. The test section is approximately 1.22 meters square and 2.13 meters long. The nozzle leading to the test section is of the asymmetric sliding-block type, which permits a continuous

variation in test-section Mach number from 2.30 to 4.63. For this investigation the tunnel stagnation temperature was 339 K at $M_\infty = 2.30$ and 2.90 and 353 K at $M_\infty = 3.95$ and 4.60. A detailed description of the facility is given in reference 5.

MODELS AND TEST PROCEDURE

The flat-plate model used in this investigation is shown in figure 1. The flat surface of the model was 36.58 cm in length, 25.40 cm in width, and had a 20° wedge leading edge. The leading-edge thickness was approximately 0.008 cm.

Cylinder drag measurements and undisturbed boundary-layer skin-friction drag measurements were obtained in separate runs using a skin-friction balance mounted in the flat plate, its sensing element being flush with the flat surface of the plate. In order to obtain the desired range of k/δ and not exceed the maximum-force limitations of the balance, it was desirable to locate the balance close to the leading edge but far enough downstream to prevent contamination from the balance cover on the opposite side of the plate feeding upstream through the boundary layer to the plate leading edge and possibly influencing the measurements. Based on these considerations, the center of the balance sensing element was located 10.16 cm from the leading edge.

The geometry and spacing of the right circular cylinders used in the investigation are shown in the table in figure 1(b). Cylinders of three different sizes were tested with the spacing between the cylinders for a given size ranging from $s/w = \infty$ (hereafter referred to as the isolated cylinder) to the approximate values of s/w that are appropriate for spacing of roughness elements used as boundary-layer trips. For the isolated-cylinder tests, a single cylinder was cemented to the balance sensing element with its longitudinal center line perpendicular to and at the center of the balance sensing element. When more than one cylinder was tested (see sketch in fig. 1(b)), the cylinders were alined in a spanwise row at right angles to the free-stream velocity vector with only one cylinder, the center cylinder, being cemented to the sensing element. The remaining cylinders were cemented to the flat surface beyond the sensing-element radius. To facilitate installation of the multicylinder configurations and to insure the correct cylinder spacing and alinement, templates were constructed and used for the cylinder installation. For the present tests a very thin film of cement applied to the cylinder base was found to be adequate for supporting the cylinders.

A cantilevered cylinder assembly used to determine the contribution from extraneous forces resulting from skin-friction drag and pressure gradients associated with the cylinder flow field on the sensing element is also shown in figure 1(b). The cantilevered cylinder was 0.127 cm in diameter, and its maximum height was 0.239 cm above the plate surface. The base of the cylinder was separated from the balancing sensing element by a 0.013-cm gap.

Shown in figure 1(c) is the pitot-probe assembly that was used to obtain pitot-pressure surveys across the boundary layer at the cylinder installation location on the flat-plate center line. For these tests, the model was rolled to a vertical position so that the flat test surface was parallel to the tunnel sidewall. The circular shaft of the pitot-probe assembly passed through the tunnel-sidewall access door and was attached to a manually operated traversing mechanism. The probe assembly was electrically insulated from the tunnel sidewall and, therefore, contact between the probe head and the plate surface could be determined by monitoring the electrical resistance between the two assemblies.

The procedure for obtaining the boundary-layer surveys consisted of first positioning the probe head against the plate surface and obtaining the pressure measurements as the probe was moved away from the plate surface. Since the measurements were always obtained with the probe being moved away from the plate surface, any inaccuracies in the probe location due to backlash in the traversing assembly are minimized.

INSTRUMENTATION AND ACCURACY

The impact-pressure measurements were obtained using a 69 kN/m^2 full-scale absolute-pressure transducer. The accuracy of this gage combined with the read-out equipment is one-half of 1 percent of full scale or ± 345 N/m^2. Free-stream stagnation pressures less than 239 kN/m^2 were measured using a precision mercury manometer with an accuracy of ± 48 N/m^2. Stagnation pressures greater than 239 kN/m^2 were measured using a 1034 kN/m^2 full-scale absolute-pressure transducer having an accuracy of one-fourth of 1 percent of full scale or ± 3 kN/m^2.

The location of the impact probe relative to the flat-plate surface is accurate to within ± 0.005 cm.

The two skin-friction balances used in this investigation utilize the force-balance principle in which the aerodynamic forces are counterbalanced by an electromagnetic force (ref. 6). A balance having a full-scale range from 0 to 0.07 newton was used for the cylinder drag measurements, whereas one having a range from 0 to 0.01 newton was used for the clean-plate skin-friction drag measurements. The accuracy of both balances was better than 1 percent of full scale.

Since the balances used in the present investigation are essentially moment-measuring devices, the balance output is proportional to the location of the applied force relative to the internal flexure point of the sensing element, which for the present balances was located 0.792 cm beneath the sensing element. If the applied resultant force is not located at the surface of the sensing element (as is the case when the balance is calibrated), a correction must be applied to the balance output to account for this discrepancy. For the case

of the cylinder drag measurements the applied force acts through the center of pressure on the cylinder, and therefore a correction must be applied to the balance output to account for the extension of the moment arm from the sensing-element surface to the cylinder center of pressure.

Based on a simplified hypothetical cylinder pressure distribution, equations are derived in appendix A for defining the variation of y_{cp}/k with k/δ. For the range of k/δ of the present investigation ($0.4 < k/\delta < 3$) calculated values of y_{cp}/k varied from 0.667 to approximately 0.58. Since this variation in y_{cp}/k of 0.087 corresponds to less than 3 percent of the total moment arm for the largest cylinder tested, an average value of y_{cp}/k of 0.62 was used in order to simplify the data-reduction procedure. Assuming the center-of-pressure location based on the assumed pressure distributions is within $\pm 0.2k$ of the actual center-of-pressure location, the maximum error in the cylinder drag-force measurement is approximately 5 percent and would occur for the cylinders having $k = 0.239$ cm. The error for the $k = 0.127$ cm cylinders would be approximately $2\frac{1}{2}$ percent.

As discussed in appendix B, the error in drag measurements for the 0.239-cm by 0.127-cm cylinder resulting from extraneous forces varied from a maximum of 3.5 percent at $M_\infty = 2.3$ to 6 percent at $M_\infty = 4.6$.

DATA REDUCTION

Boundary-Layer Profile Data

From measured pitot-pressure surveys across the boundary layer, nondimensionalized velocity distributions were calculated using the following equation:

$$\frac{u}{u_\infty} = \frac{M}{M_\infty} \frac{\sqrt{1 + \frac{\gamma - 1}{2} M_\infty^2}}{\sqrt{1 + \frac{\gamma - 1}{2} M^2}} \tag{1}$$

where M was obtained from the pitot-probe pressure measurements and free-stream static pressure (which was assumed to remain constant across the boundary layer) substituted into Rayleigh's pitot formula. The stagnation temperature was also assumed to remain constant across the boundary layer.

Boundary-layer displacement thicknesses were calculated from the following equation:

$$\delta^* = \int_0^{\delta} \left[1 - \frac{u}{u_\infty} \left(\frac{1 - \frac{\gamma - 1}{2} M^2}{1 + \frac{\gamma - 1}{2} M_\infty^2} \right) \right] dy \tag{2}$$

The boundary-layer thickness δ was assumed to be the value of y at which the measured velocity was 0.995 of the local velocity at the boundary-layer edge.

Cylinder Drag Force Measurements

As discussed previously, the variation of y_{cp}/k with k/δ for the range of k/δ of the present investigation was found to be small relative to the moment arm from the sensing-element hinge point to the calculated center-of-pressure location. A constant value of $y_{cp}/k = 0.62$ was therefore used to correct the balance output and was applied in the form of the following equality:

$$(\text{Drag force})_{\text{Corrected}} = (\text{Drag force})_{\text{Measured}} \left(\frac{0.792}{0.62k + 0.792} \right) \tag{3}$$

The cylinder drag coefficients were then obtained from the following equation:

$$C_D = \frac{(\text{Drag force})_{\text{Corrected}}}{q_\infty A} \tag{4}$$

where q_∞ is free-stream dynamic pressure and A is the cylinder frontal area.

RESULTS AND DISCUSSION

Boundary-Layer Surveys

In order to insure that the boundary layer on the flat plate at the cylinder installation location was a well-behaved, typical, laminar boundary layer, pitot-pressure surveys were obtained on the flat-plate center line through the range of Reynolds numbers and Mach numbers for which cylinder drag measurements were obtained. Presented in figure 2 is a typical velocity profile computed from the pitot-pressure measurements, assuming constant total temperature and constant static pressure through the boundary layer. The distortion

of the profile due to the finite probe size is readily apparent near the plate surface. In order to minimize this probe effect on the calculation of boundary-layer displacement thickness to be presented subsequently, a linear variation in u/u_∞ with y was assumed from the flat-plate surface to the approximate location of the inflection point in the measured profile. This assumption as shown in figure 2 results in a velocity distribution as indicated by the flagged symbols that is in good agreement with the theoretical profile of reference 7. A complete listing of measured velocity distributions through the boundary layer corrected in the vicinity of the plate surface as discussed are tabulated in table I for the range of test variables.

Experimental velocity profiles in which the distance off the plate surface has been nondimensionalized by the boundary-layer displacement thickness are presented in figure 3. These results are compared with the theoretical profiles of references 7 and 8. The measured profiles are generally in good agreement with the theory of reference 7 through the range of test Mach numbers and Reynolds numbers. The theory of reference 8 overpredicts the velocities for a given value of y/δ^* with the extent of disagreement increasing with increasing Mach number (figs. 3(a) to 3(d)). The good agreement of the experimental profile with the more exact theory of reference 7 indicates that any effects of leading-edge bluntness or finite aspect ratio on the flat-plate laminar boundary layer at the location of the center cylinder installation are minimal.

Presented in figure 4 are comparisons of boundary-layer thicknesses determined from experimental velocity profiles with theoretical values from references 7 and 8. The experimental values and theoretical values from reference 7 correspond to values of $\frac{u}{u_\ell} = 0.995$, whereas the results from reference 8 correspond to a value of $\frac{u}{u_\ell} = 1.0$. In general, good agreement is shown between experiment and the theory of reference 7, whereas the theory of reference 8 underpredicts the experimental values. The extent of this disagreement decreases with increasing Mach number.

Boundary-layer displacement thicknesses calculated from equation (2) using experimental profiles are compared in figure 5 with theoretical values from references 7 and 8. The experimental values of δ^* were calculated with the assumption of the linear velocity profiles in the near wall region, as discussed previously. The maximum percentage difference between the values obtained using this assumption and the values determined from integrating the experimental profiles from the boundary-layer edge to the model wall was approximately 3 percent. Fair agreement is shown in figure 5 between experiment and both theories for the range of test variables. Values of δ^* used for nondimensionalizing cylinder height for subsequent cylinder-drag presentations were obtained from the solid lines faired through the experimental data.

Clean-Plate Skin-Friction Balance Measurements

Skin-friction coefficients calculated from the "clean-plate" skin-friction balance measurements are presented in figure 6 for the range of test variables. Also presented are values determined from the assumed linear velocity profiles in the wall region as well as theoretical values from several theories. The values of c_f determined from the skin-friction balance measurements and velocity profiles are generally in good agreement through the range of test variables. The theories of references 7, 8, and 9 are in good agreement with the experimental data for the range of test conditions. The theory of reference 10 is in good agreement with experiment at the lower Mach numbers but underpredicts the experimental values at the higher Mach numbers.

Cylinder Drag Measurements

Drag coefficients determined from balance measurements for the isolated-cylinder configurations are presented in figure 7. Results are shown in figure 7(a) for cylinders having equal diameters and heights ($k = w$), whereas the results shown in figure 7(b) are for a cylinder having a height approximately twice its diameter ($k \approx 2w$). For all the experimental data shown in figure 7, the values of δ^* used to nondimensionalize k on the abscissa scale were obtained from the data fairings presented in figure 5.

Experimental results are presented in figure 7(a) for cylinders of two different diameters, 0.127 cm and 0.239 cm, as indicated by the flagged and unflagged symbols, respectively. When the drag coefficients are plotted as a function of k/δ^* as shown, the data fall into a narrow band for the test range of Mach number and cylinder diameter.

Also shown in figure 7 are approximate theoretical calculations for $M_\infty = 2.30$ and 4.60 based on the following assumptions:

(1) The pressure distribution along the stagnation line of the segment of the cylinder submerged within the laminar boundary layer corresponds to the local pitot pressure across the boundary layer.

(2) The stagnation-line pressure on the segment of the cylinder external to the boundary layer corresponds to the free-stream pitot pressure.

(3) The circumferential pressure-coefficient distribution around the cylinder varies as

$$C_p = C_{p_{SL}} \cos^2\theta \qquad (270^\circ \leq \theta \leq 90^\circ)$$

where θ is the angle between the unit normal vector on the cylinder surface and the free-stream velocity vector.

(4) The base pressure coefficients over the rear half of the cylinder ($90° \leq \theta \leq 270°$) are assumed to be invariant with θ and to vary linearly with y from a value of $C_{p,b} = 0$ at the plate surface to a value of $C_{p,b} = -\frac{1}{M_\infty^2}$ at the boundary-layer edge. For values of $\delta < y \leq k$, the base pressure coefficient is assumed to remain constant at $C_{p,b} = -\frac{1}{M_\infty^2}$ (ref. 11).

Based on these assumptions, the following equations were derived to define the cylinder drag coefficients:

$$C_D = \frac{2}{3}\frac{1}{q_\infty/p_\infty}\left[\frac{\delta}{k}\int_0^{k/\delta}\frac{p_{SL}}{p_\infty}\,d\left(\frac{y}{\delta}\right) - 1\right] + \frac{1}{2}\frac{k}{\delta}\left(\frac{1}{M_\infty^2}\right) \qquad \left(\frac{k}{\delta} \leq 1\right) \qquad (5)$$

$$C_D = \frac{2}{3}\frac{1}{q_\infty/p_\infty}\left[\frac{p_{t,2}}{p_\infty}\left(1 - \frac{\delta}{k}\right) - 1 + \frac{\delta}{k}\int_0^1 \frac{p_{SL}}{p_\infty}\,d\left(\frac{y}{\delta}\right)\right] + \frac{1}{M_\infty^2}\left[1 - \frac{1}{2\left(\frac{k}{\delta}\right)}\right] \qquad \left(\frac{k}{\delta} > 1\right) \qquad (6)$$

Calculations from equations (5) and (6) are generally in good agreement with experimental data for the cylinders having $k \approx 2w$ (fig. 7(b)) but tend to overestimate the experimental drag coefficients for the cylinders with $k = w$ (fig. 7(a)). The small effect of Mach number on the variation of C_D with k/δ^* shown by both sets of experimental data is also indicated by the theoretical calculations. The reduction in drag coefficient with decreasing k/w as indicated by the experimental data is believed to be associated with the effects of k/w on the extent of boundary-layer separation ahead of the cylinder. Since the effects of separation on the cylinder pressure distribution are unknown, no attempt was made to account for these effects on the hypothetical cylinder pressure distribution. With increasing k/w, however, the extent of separation ahead of the cylinder would be expected to decrease and result in an improvement between experiment and theory, which is the trend shown in figure 7.

Before results such as presented in figure 7 for isolated cylinders can be applied to determine the drag of small cylinders used as boundary-layer trips, it is necessary to establish the effect on the isolated-cylinder drag of adding additional cylinders in its proximity. In order to determine this effect, additional cylinders were installed on the flat-plate surface alined in a spanwise row on both sides of the instrumented cylinder and perpendicular to the free-stream velocity vector. Drag measurements were obtained through a range of cylinder spacings (fig. 1(b)).

Presented in figure 8 are typical measured drag coefficients for a cylinder located in a spanwise row of cylinders for Mach numbers of 2.30 and 3.95. The results are presented for the cylinders having $k \approx 2w$ and for values of s/w ranging from 5 to ∞, the latter case corresponding to the isolated cylinder. In general, increasing the distance between cylinders results in an increase in cylinder drag coefficient. The similarity between the trend of the variation of C_D with k/δ^* for the row of cylinders and the isolated cylinder suggests that a drag-coefficient parameter of the form $C_D/C_{D_{IC}}$, where the two drag coefficients are evaluated at equal values of k/δ^*, would not be as sensitive to k/δ^* as the individual values. This normalized drag-coefficient parameter was determined for the complete range of cylinder and free-stream variables, and the results are presented in figures 9 to 11. These results indicate that, for values of $k/\delta^* \gtrapprox 2.0$, the normalized drag coefficients are essentially independent of k/δ^*. For values of $k/\delta^* < 2.0$, the normalized values generally approach a value of 1 which would be expected since the interference created by adjacent cylinders would tend to be minimized as k/δ^* approaches zero. The magnitude of the normalized drag coefficients for $k/\delta^* > 2$ tends to decrease with increasing Mach number and to increase with increasing s/w. At the higher supersonic Mach numbers, tripping elements greater in height than the boundary-layer thickness are required to move transition to the vicinity of the element (refs. 2 and 3). Since the value of $\frac{k}{\delta^*} = 2$ corresponds to values of $\frac{k}{\delta} \approx 1.0$ at $M_\infty = 2.3$ and $\frac{k}{\delta} \approx 1.4$ at $M_\infty = 4.60$, normalized drag coefficients for cylinders used as boundary-layer trips should be either near or in the range of k/δ^* where the values of $C_D/C_{D_{IC}}$ are independent of k/δ^*.

The approximate level of the normalized drag coefficients for $k/\delta^* > 2$ is cross-plotted in figure 12 in order to illustrate the effects of cylinder size, spacing, and Mach number better. As shown in figure 12, the data for all cylinders tested collapse into a narrow band at each test Mach number and indicate a decrease in drag with decreasing s, as previously noted. The effect of Mach number on the normalized drag coefficients, which consists of a decrease in drag with an increase in Mach number, can be more clearly seen in figure 12(b) where the curves representing experimental data fairings at each Mach number from figure 12(a) are plotted relative to a common origin. In order to determine the drag coefficient for a given cylinder configuration used as a boundary-layer trip, therefore, the following simple procedure using the present results can be utilized provided (a) $\frac{k}{\delta^*} \gtrapprox 2$, (b) $1 \leqq \frac{k}{w} \lessapprox 2$, (c) $2.3 \leqq M_\ell \leqq 4.6$, and (d) the cylinders are alined in a spanwise row perpendicular to the free-stream velocity vector:

(1) Evaluate $C_D/C_{D_{IC}}$ from figure 12(b) for given values of M_ℓ and w/s

(2) Evaluate $C_{D_{IC}}$ from figure 7 for given values of k/δ^* and k/w

CONCLUDING REMARKS

An experimental investigation has been conducted to define drag coefficients for circular cylinders mounted on a flat-plate surface having a laminar boundary layer. The cylinders were alined in a spanwise row perpendicular to the free-stream velocity vector. The drag measurements were obtained through a range of

(a) Mach number from 2.3 to 4.6

(b) Spacing s between cylinders ranging from an isolated cylinder $\left(\frac{s}{w} = \infty\right.$, where w is the cylinder diameter$\left.\right)$ to spacings appropriate for boundary-layer trips

(c) Cylinder heights k ranging from approximately 0.4 to 3 times the undisturbed laminar boundary-layer thickness

(d) Cylinder height-to-diameter ratios of 1.0 and approximately 2

The results of this investigation lead to the following concluding remarks:

1. The isolated-cylinder drag coefficient $\left(\frac{s}{w} = \infty\right)$ when plotted as a function of the ratio of cylinder height to boundary-layer displacement thickness, k/δ^*, was found to be only a weak function of free-stream Mach number and k/w. These results for the cylinder with a height-to-diameter ratio of approximately 2 are in good agreement with results from an approximate theoretical calculation based on a hypothetical cylinder pressure distribution described in the test.

2. Decreasing spacing between cylinders resulted in a decrease in cylinder drag coefficients.

3. Increasing k/δ^* resulted in an increase in cylinder drag coefficient; however, if the cylinder drag coefficients for the row of cylinders are normalized by the isolated-cylinder values, the normalized parameter is essentially invariant with $\frac{k}{\delta^*}$ for $\frac{k}{\delta^*} \gtrsim 2$.

4. A simplified procedure is outlined in the text for obtaining cylinder drag coefficients using the results of this investigation.

5. Results obtained from impact-pressure surveys through the laminar boundary layer on the center line of the flat-plate surface were in good agreement with the theory of NASA TR R-368.

Langley Research Center,
National Aeronautics and Space Administration,
Hampton, Va., September 26, 1973.

APPENDIX A

ESTIMATE OF CENTER-OF-PRESSURE LOCATION ON A CIRCULAR CYLINDER ATTACHED TO A FLAT PLATE HAVING A LAMINAR BOUNDARY LAYER

Since the skin-friction balance used to measure cylinder drag in the present investigation is essentially a moment-measuring instrument, it is necessary to define the location at which the resultant drag force acts on the cylinder so that the correct moment arm can be determined. If the pressure distribution over the cylinder can be defined, the center-of-pressure location can be obtained from the following equation:

$$y_{cp} = \frac{(\text{Moment})_{y=0}}{\text{Drag force}} \tag{A1}$$

Using the following sketch illustrating the cylinder orientation and incremental areas,

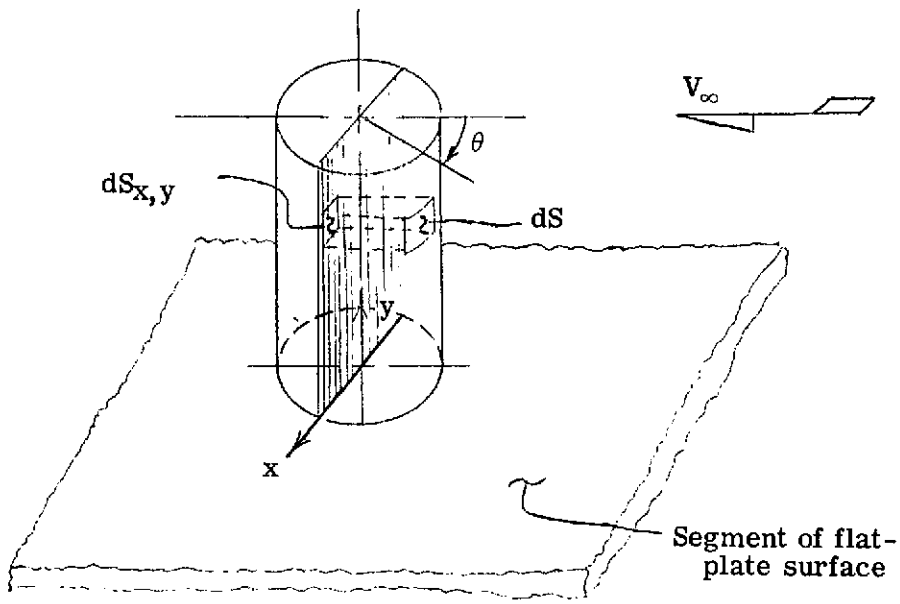

Sketch A1

the moment about the cylinder base ($y = 0$) and the cylinder drag force can be expressed as integrals of the local surface pressure acting on the surface-area projection in the x,y planes as follows:

$$(\text{Moment})_{y=0} = \iint_S py \, dS_{xy} \tag{A2}$$

$$\text{Drag force} = \iint_S p \, dS_{xy} \tag{A3}$$

At present, no exact method exists for predicting the pressure distribution over a cylinder protruding through a laminar boundary layer; therefore, in order to evaluate the integrals of equations (A2) and (A3), the following hypothetical pressure distribution was assumed:

(1) The pressure distribution along the cylinder stagnation line varies as shown in the following sketch:

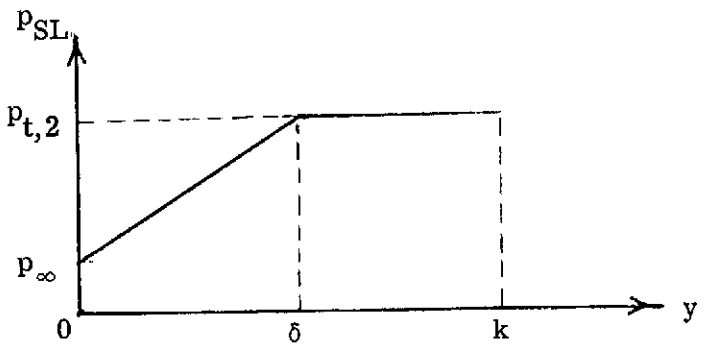

Sketch A2

resulting in the following equations for cases where $k > \delta$:

$$p_{SL} = p_\infty + \frac{p_{t,2} - p_\infty}{\delta} y \qquad (y \leq \delta) \tag{A4}$$

$$p_{SL} = p_{t,2} \qquad (y > \delta) \tag{A5}$$

(2) For $270° \leq \theta \leq 90°$, the pressure coefficient varies as $\cos^2\theta$ and, as a result, the following equations are obtained:

$$p = p_\infty + (p_{t,2} - p_\infty) \frac{y}{\delta} \cos^2\theta \qquad (y \leq \delta) \tag{A6}$$

$$p = p_\infty + (p_{t,2} - p_\infty) \cos^2\theta \qquad (y > \delta) \tag{A7}$$

(3) The base pressure coefficients over the rear half of the cylinder ($90° \leq \theta \leq 270°$) are assumed to be invariant with θ and to vary linearly with y from a value of $C_{p,b} = 0$ at the plate surface to a value of $C_{p,b} = -\frac{1}{M_\infty^2}$ at the boundary-layer edge. For values of $\delta < y \leq k$, the base pressure coefficient is assumed to remain constant at a value $C_{p,b} = -\frac{1}{M_\infty^2}$.

It should be noted that assumptions 2 and 3 are the same assumptions used in the main text for the circumferential and base pressure distributions in the derivation of equations (5) and (6). The assumption used in this appendix for the stagnation line pressure ($0 \leq y \leq \delta$), however, is a more simplified approximation than that used in the derivation of equations (5) and (6). Since the linear variation in pressure assumed here results in a closed-form solution for y_{cp} and since the distance from the plate surface to y_{cp} is only a small fraction of the total moment arm from the balance moment center, it is believed that this more simplified approach is justified for the purpose of calculating the center-of-pressure location.

Substituting equations (A4) through (A7) into the integral equations for moment and drag force and expressing the incremental area in polar coordinates results in the following set of equations for $k \geq \delta$:

$$(\text{Moment})_{y=0} = 2\int_0^{\delta}\int_0^{\pi/2}\left[p_\infty + (p_{t,2} - p_\infty)\frac{y}{\delta}\cos^2\theta\right] yr\cos\theta\, d\theta\, dy$$

$$+ 2\int_{\delta}^{k}\int_0^{\pi/2}\left[p_\infty + (p_{t,2} - p_\infty)\cos^2\theta\right] yr\cos\theta\, d\theta\, dy$$

$$- p_\infty rk^2 - r\delta^2 p_\infty + \frac{2r\delta^2}{3}\frac{q_\infty}{M_\infty^2} - r(k+\delta)(k-\delta)\left(p_\infty - \frac{q_\infty}{M_\infty^2}\right) \qquad \text{(A8)}$$

$$\text{Drag force} = 2\int_0^{\delta}\int_0^{\pi/2}\left[p_\infty + (p_{t,2} - p_\infty)\frac{y}{\delta}\cos^2\theta\right] r\cos\theta\ d\theta\ dy$$

$$+ 2\int_{\delta}^{k}\int_0^{\pi/2}\left[p_\infty + (p_{t,2} - p_\infty)\cos^2\theta\right] r\cos\theta\ d\theta\ dy$$

$$- r\delta\frac{q_\infty}{M_\infty^2} - 2rkp_\infty + 2rk\frac{q_\infty}{M_\infty^2} \tag{A9}$$

Equations (A8) and (A9) can be integrated to obtain the following equations:

$$(\text{Moment})_{y=0} = \frac{2}{9}r\delta^2(p_\infty - p_{t,2}) - \frac{2}{3}rk^2(p_\infty - p_{t,2}) \tag{A10}$$

$$\text{Drag force} = \frac{2}{3}\delta r(p_\infty - p_{t,2}) - \frac{4}{3}rk(p_\infty - p_{t,2}) \tag{A11}$$

Substituting equations (A10) and (A11) into equation (A1) gives the following equation for the center-of-pressure location:

$$\frac{y_{cp}}{k} = \frac{\frac{1}{3} - \left(\frac{k}{\delta}\right)^2}{\frac{k}{\delta} - 2\left(\frac{k}{\delta}\right)^2} \qquad \left(k \geq \delta\right) \tag{A12}$$

For cylinder heights less than the boundary-layer thickness, it can be readily shown that the center-of-pressure location for the hypothetical pressure distribution is

$$\frac{y_{cp}}{k} = \frac{2}{3} \qquad \left(k \leq \delta\right) \tag{A13}$$

The variation of y_{cp}/k with k/δ is shown in figure 13 for the approximate k/δ range of the present investigation.

APPENDIX B

CANTILEVERED-CYLINDER MEASUREMENTS

In order to assess the error in cylinder drag measurements associated with extraneous forces resulting from skin-friction drag and pressure gradients acting on the balance sensing element, a cantilevered-cylinder arrangement (see fig. 1(b)) was tested where only the extraneous forces were applied to the balance. Results obtained from these measurements are presented in figure 14 and are compared with cylinder drag measurements obtained for the 0.239 cm by 0.127 cm cylinder. Through the range of Mach number (figs. 14(a) to 14(d)), the extraneous force measurements obtained using the cantilevered cylinder are over an order of magnitude less than the total drag measurements obtained with the cylinder attached to the sensing element. The maximum percentage error in the total drag measurement resulting from these extraneous forces as determined from these results varies from approximately 3 percent at $M_\infty = 2.30$ to 6 percent at $M_\infty = 4.60$.

At the two lower test Mach numbers, an anomalous behavior occurred in the variation of the extraneous forces with Reynolds number at the higher Reynolds numbers. This anomaly consists of a decrease in the measured extraneous forces with an increase in Reynold number; for example, at $M_\infty = 2.30$ (fig. 14(a)), increasing R from 0.5×10^6 to 0.67×10^6 results in a force reduction from approximately 0.0013 N to a value that was actually negative. Since the balance was not calibrated for negative forces and, also, since a negative force cannot be shown on the log coordinate of figure 14, this result is not presented. At $M_\infty = 2.90$ (fig. 14(b)), increasing R from 0.77×10^6 to 0.83×10^6 resulted in an approximate 25-percent force reduction. This anomaly was not observed at the two higher Mach numbers.

This anomalous behavior in the extraneous forces is believed to result from the location of boundary-layer transition, induced by the cylinder, moving forward to the immediate proximity or possibly even ahead of the cylinder and influencing the forced separation in this region. This hypothesis is substantiated by voltage fluctuation measurements obtained (although not presented herein) using a thin-film heat-flux gage that was located immediately upstream of a 0.239 cm by 0.127 cm cylinder mounted on a dummy balance and located at the same position on the flat plate as the cylinders used for the drag measurements. The dummy balance was machined to house the heat-flux gage so that the thin film was flush with the plate surface. Additional heat-flux gages were located on the plate center line downstream of the cylinder to establish the rms voltage fluctuation level typical of a turbulent boundary layer for these test conditions. Measurements were obtained only at a Mach number of 2.3. For Reynolds numbers $\leq 0.47 \times 10^6$ the rms voltage fluctuations from the gage ahead of the cylinder were approximately an order of magnitude less than values obtained downstream of the cylinder where the boundary layer

was turbulent. At $R \approx 0.5 \times 10^6$ the rms voltage fluctuation measurements ahead of the cylinder abruptly increased to values even greater than those obtained downstream of the cylinder; however, with a further increase in Reynolds number the fluctuation measurements rapidly approached the downstream values. The trend of the variation of the rms voltage fluctuations with Reynolds number ahead of the cylinder is typical of the fluctuation associated with a boundary layer going from laminar to transitional and, finally, to turbulent conditions as reported in reference 12.

REFERENCES

1. Braslow, Albert L.; Hicks, Raymond M.; and Harris, Roy V., Jr.: Use of Grit-Type Boundary-Layer-Transition Trips on Wind-Tunnel Models. NASA TN D-3579, 1966.
2. Potter, J. Leith; and Whitfield, Jack D.: Effects of Unit Reynolds Number, Nose Bluntness, and Roughness on Boundary Layer Transition. AEDC-TR-60-5, U.S. Air Force, Mar. 1960.
3. Sterrett, James R.; Morrisette, E. Leon; Whitehead, Allen H., Jr.; and Hicks, Raymond M.: Transition Fixing for Hypersonic Flow. NASA TN D-4129, 1967.
4. Whitehead, Allen H., Jr.: Flow-Field and Drag Characteristics of Several Boundary-Layer Tripping Elements in Hypersonic Flow. NASA TN D-5454, 1969.
5. Anon.: Manual for Users of the Unitary Plan Wind Tunnel Facilities of the National Advisory Committee for Aeronautics. NACA, 1956.
6. Paros, Jerome M.: Application of the Force-Balance Principle to Pressure and Skin Friction Sensors. 16th Annual Technical Meeting Proceedings, Inst. Environ. Sci., 1970, pp. 363-368.
7. Harris, Julius E.: Numerical Solution of the Equations for Compressible Laminar, Transitional, and Turbulent Boundary Layers and Comparisons With Experimental Data. NASA TR R-368, 1971.
8. Monaghan, R. J.: An Approximate Solution of the Compressible Laminar Boundary Layer on a Flat Plate. R. & M. No. 2760, Brit. A.R.C., 1953.
9. Chapman, Dean R.; and Rubesin, Morris W.: Temperature and Velocity Profiles in the Compressible Laminar Boundary Layer With Arbitrary Distribution of Surface Temperature. J. Aeronaut. Sci., vol. 16, no. 9, Sept. 1949, pp. 547-565.
10. Van Driest, E. R.: Investigation of Laminar Boundary Layer in Compressible Fluids Using the Crocco Method. NACA TN 2597, 1952.
11. Stallings, Robert L., Jr.: Experimentally Determined Local Flow Properties and Drag Coefficients for a Family of Blunt Bodies at Mach Numbers from 2.49 to 4.63. NASA TR R-274, 1967.
12. Owen, F. K.: Transition Experiments on a Flat Plate at Subsonic and Supersonic Speeds. AIAA J., vol. 8, no. 3, Mar. 1970, pp. 518-523.

TABLE I.- TABULATED RESULTS FROM PITOT SURVEYS

(a) M = 2.30

$R = 0.20 \times 10^6$ $\delta^* = 0.0940$ cm		$R = 0.33 \times 10^6$ $\delta^* = 0.0752$ cm		$R = 0.50 \times 10^6$ $\delta^* = 0.0615$ cm		$R = 0.67 \times 10^6$ $\delta^* = 0.0526$ cm		$R = 1.00 \times 10^6$ $\delta^* = 0.0457$ cm	
y/δ^*	u/u_∞	y/δ^*	u/u_∞	y/δ^*	u/u_∞	y/δ^*	u/u_∞	y/δ^*	u/u_∞
0.095	0.0738	0.118	0.0906	0.145	0.1192	0.169	0.1335	0.194	0.1607
0.230	0.1792	0.287	0.2201	0.351	0.2896	0.411	0.3241	0.472	0.3902
0.365	0.2846	0.456	0.3495	0.558	0.4599	0.652	0.5147	0.750	0.6197
0.419	0.3268	0.524	0.4013	0.640	0.5281	0.749	0.5910	0.861	0.6692
0.473	0.3690	0.591	0.4531	0.723	0.5962	0.845	0.6494	0.972	0.7254
0.527	0.4111	0.659	0.5048	0.806	0.6426	0.942	0.7005	1.083	0.7861
0.581	0.4533	0.726	0.5566	0.888	0.6833	1.039	0.7621	1.194	0.8363
0.635	0.4955	0.794	0.6084	0.971	0.7287	1.135	0.8054	1.306	0.8793
0.689	0.5376	0.861	0.6486	1.054	0.7751	1.232	0.8505	1.417	0.9148
0.743	0.5798	0.929	0.6894	1.136	0.8194	1.329	0.8889	1.528	0.9435
0.797	0.6051	0.997	0.7280	1.219	0.8520	1.425	0.9162	1.639	0.9589
0.851	0.6374	1.064	0.7670	1.302	0.8804	1.522	0.9412	1.750	0.9734
0.905	0.6630	1.132	0.7991	1.384	0.9091	1.618	0.9569	1.861	0.9823
0.959	0.6933	1.199	0.8360	1.467	0.9301	1.715	0.9719	1.972	0.9874
1.014	0.7273	1.267	0.8609	1.550	0.9501	1.812	0.9808	2.083	0.9904
1.068	0.7566	1.334	0.8887	1.632	0.9620	1.908	0.9868	2.194	0.9927
1.122	0.7868	1.402	0.9073	1.715	0.9723	2.005	0.9905		
1.176	0.8149	1.470	0.9280	1.798	0.9787	2.101	0.9927		
1.230	0.8381	1.537	0.9438	1.880	0.9864				
1.284	0.8637	1.605	0.9567	1.963	0.9893				
1.338	0.8822	1.672	0.9666	2.045	0.9916				
1.392	0.9010	1.740	0.9750	2.128	0.9937				
1.446	0.9173	1.807	0.9824						
1.500	0.9335	1.875	0.9863						
1.554	0.9468	1.943	0.9896						
1.608	0.9569	2.010	0.9921						
1.662	0.9660	2.078	0.9937						
1.716	0.9729								
1.770	0.9790								
1.824	0.9836								
1.878	0.9871								
1.932	0.9900								
1.986	0.9921								
2.041	0.9937								

TABLE I.- TABULATED RESULTS FROM PITOT SURVEYS – Continued

(b) M = 2.90

$R = 0.20 \times 10^6$ $\delta^* = 0.1151$ cm		$R = 0.33 \times 10^6$ $\delta^* = 0.0902$ cm		$R = 0.67 \times 10^6$ $\delta^* = 0.0681$ cm		$R = 1.00 \times 10^6$ $\delta^* = 0.0551$ cm		$R = 1.33 \times 10^6$ $\delta^* = 0.0516$ cm	
y/δ^*	u/u_∞	y/δ^*	u/u_∞	y/δ^*	u/u_∞	y/δ^*	u/u_∞	y/δ^*	u/u_∞
0.077	0.0638	0.099	0.0816	0.131	0.1072	0.161	0.1360	0.172	0.1518
0.188	0.1549	0.239	0.1983	0.317	0.2604	0.392	0.3302	0.419	0.3686
0.298	0.2461	0.380	0.3149	0.504	0.4136	0.622	0.5245	0.665	0.5855
0.342	0.2825	0.437	0.3616	0.578	0.4749	0.714	0.5824	0.764	0.6550
0.386	0.3190	0.493	0.4082	0.653	0.5362	0.806	0.6416	0.862	0.7206
0.430	0.3554	0.549	0.4549	0.728	0.5844	0.899	0.7017	0.961	0.7802
0.475	0.3919	0.606	0.5015	0.802	0.6363	0.991	0.7634	1.059	0.8417
0.519	0.4283	0.662	0.5482	0.877	0.6831	1.083	0.8136	1.158	0.8839
0.563	0.4648	0.718	0.5826	0.951	0.7393	1.175	0.8647	1.256	0.9209
0.607	0.5012	0.775	0.6238	1.026	0.7855	1.267	0.9029	1.355	0.9475
0.651	0.5377	0.831	0.6604	1.101	0.8259	1.359	0.9305	1.453	0.9694
0.695	0.5714	0.887	0.6977	1.175	0.8681	1.452	0.9555	1.552	0.9799
0.740	0.6040	0.944	0.7385	1.250	0.8972	1.544	0.9709	1.650	0.9896
0.784	0.6268	1.000	0.7730	1.325	0.9240	1.636	0.9839	1.749	0.9936
0.828	0.6588	1.056	0.8040	1.399	0.9431	1.728	0.9906	1.847	0.9962
0.872	0.6917	1.113	0.8339	1.474	0.9608	1.820	0.9952		
0.916	0.7204	1.169	0.8591	1.549	0.9747				
0.960	0.7499	1.225	0.8824	1.623	0.9833				
1.004	0.7763	1.282	0.9030	1.698	0.9897				
1.049	0.8012	1.338	0.9237	1.772	0.9928				
1.093	0.8272	1.394	0.9392	1.847	0.9953				
1.137	0.8510	1.451	0.9537						
1.181	0.8711	1.507	0.9650						
1.225	0.8880	1.563	0.9747						
1.269	0.9066	1.620	0.9820						
1.313	0.9213	1.676	0.9872						
1.358	0.9354	1.732	0.9914						
1.402	0.9479	1.789	0.9942						
1.446	0.9572	1.845	0.9963						
1.490	0.9650								
1.534	0.9724								
1.548	0.9788								
1.623	0.9846								
1.667	0.9882								
1.711	0.9912								
1.755	0.9940								
1.799	0.9959								

TABLE I.- TABULATED RESULTS FROM PITOT SURVEYS – Continued

(c) M = 3.95

$R = 0.27 \times 10^6$ $\delta^* = 0.1585$ cm		$R = 0.50 \times 10^6$ $\delta^* = 0.1234$ cm		$R = 0.67 \times 10^6$ $\delta^* = 0.1064$ cm		$R = 1.00 \times 10^6$ $\delta^* = 0.0869$ cm	
y/δ^*	u/u_∞	y/δ^*	u/u_∞	y/δ^*	u/u_∞	y/δ^*	u/u_∞
0.056	0.0479	0.072	0.0635	0.084	0.0739	0.102	0.0908
0.136	0.1164	0.175	0.1541	0.203	0.1795	0.249	0.2205
0.216	0.1849	0.278	0.2448	0.322	0.2851	0.395	0.3502
0.280	0.2397	0.360	0.3173	0.370	0.3273	0.453	0.4020
0.345	0.2945	0.442	0.3898	0.418	0.3695	0.512	0.4539
0.409	0.3493	0.525	0.4623	0.465	0.4117	0.570	0.5058
0.473	0.4040	0.566	0.4986	0.513	0.4540	0.629	0.5482
0.537	0.4588	0.607	0.5275	0.561	0.4962	0.687	0.5925
0.601	0.5136	0.648	0.5558	0.609	0.5312	0.746	0.6388
0.665	0.5684	0.689	0.5911	0.656	0.5676	0.804	0.6870
0.729	0.6193	0.730	0.6194	0.704	0.6043	0.863	0.7307
0.793	0.6707	0.772	0.6521	0.752	0.6418	0.921	0.7727
0.857	0.7172	0.813	0.6839	0.800	0.6826	0.980	0.8104
0.921	0.7611	0.854	0.7170	0.847	0.7207	1.038	0.8454
0.986	0.8031	0.895	0.7467	0.895	0.7544	1.096	0.8801
1.050	0.8419	0.936	0.7773	0.943	0.7844	1.155	0.9095
1.114	0.8780	0.977	0.8035	0.990	0.8167	1.213	0.9354
1.178	0.9100	1.019	0.8282	1.038	0.8441	1.272	0.9551
1.242	0.9386	1.060	0.8546	1.086	0.8741	1.330	0.9706
1.306	0.9620	1.101	0.8790	1.134	0.8984	1.389	0.9825
1.370	0.9773	1.142	0.8992	1.181	0.9215	1.447	0.9902
1.434	0.9882	1.183	0.9199	1.229	0.9419	1.505	0.9948
1.498	0.9941	1.224	0.9377	1.277	0.9578	1.564	0.9969
1.563	0.9978	1.265	0.9524	1.325	0.9708		
		1.307	0.9672	1.372	0.9811		
		1.348	0.9779	1.420	0.9881		
		1.389	0.9837	1.468	0.9924		
		1.430	0.9900	1.516	0.9952		
		1.471	0.9934				
		1.512	0.9959				

TABLE I.- TABULATED RESULTS FROM PITOT SURVEYS – Concluded

(d) M = 4.60

$R = 0.27\times10^6$ $\delta^* = 0.2139$ cm		$R = 0.33\times10^6$ $\delta^* = 0.1935$ cm		$R = 0.50\times10^6$ $\delta^* = 0.1613$ cm		$R = 0.67\times10^6$ $\delta^* = 0.1422$ cm		$R = 1.00\times10^6$ $\delta^* = 0.1181$ cm		$R = 1.33\times10^6$ $\delta^* = 0.1044$ cm	
y/δ^*	u/u_∞	y/δ^*	u/u_∞	y/δ^*	u/u_∞	y/δ^*	u/u_∞	y/δ^*	u/u_∞	y/δ^*	u/u_∞
0.042	0.0373	0.046	0.0410	0.055	0.0485	0.063	0.0554	0.075	0.0689	0.085	0.0778
0.101	0.0907	0.112	0.0996	0.134	0.1178	0.152	0.1347	0.183	0.1674	0.207	0.1889
0.160	0.1441	0.177	0.1583	0.213	0.1871	0.241	0.2139	0.290	0.2659	0.328	0.3000
0.208	0.1867	0.230	0.2052	0.276	0.2425	0.313	0.2772	0.376	0.3447	0.377	0.3445
0.255	0.2294	0.282	0.2520	0.339	0.2980	0.384	0.3406	0.462	0.4235	0.426	0.3889
0.303	0.2721	0.335	0.2989	0.402	0.3534	0.455	0.4040	0.548	0.5023	0.474	0.4334
0.350	0.3148	0.387	0.3458	0.465	0.4088	0.527	0.4673	0.591	0.5417	0.523	0.4778
0.398	0.3575	0.440	0.3927	0.528	0.4643	0.598	0.5307	0.634	0.5836	0.572	0.5223
0.445	0.4002	0.492	0.4396	0.591	0.5197	0.634	0.5624	0.677	0.6231	0.620	0.5621
0.493	0.4428	0.545	0.4865	0.654	0.5795	0.670	0.5986	0.720	0.6597	0.669	0.6013
0.540	0.4855	0.597	0.5334	0.685	0.6024	0.705	0.6291	0.763	0.6962	0.718	0.6422
0.588	0.5282	0.650	0.5740	0.717	0.6293	0.741	0.6607	0.806	0.7305	0.766	0.6864
0.635	0.5634	0.702	0.6184	0.748	0.6534	0.777	0.6925	0.849	0.7626	0.815	0.7272
0.683	0.6043	0.755	0.6673	0.780	0.6848	0.813	0.7191	0.892	0.7950	0.864	0.7662
0.730	0.6437	0.807	0.7066	0.811	0.7118	0.848	0.7472	0.935	0.8246	0.912	0.7972
0.778	0.6792	0.860	0.7469	0.843	0.7336	0.884	0.7736	0.978	0.8515	0.961	0.8349
0.825	0.7172	0.912	0.7858	0.874	0.7577	0.920	0.8001	1.022	0.8789	1.010	0.8680
0.873	0.7549	0.965	0.8236	0.906	0.7816	0.955	0.8246	1.065	0.9054	1.058	0.8912
0.920	0.7907	1.017	0.8594	0.937	0.8037	0.991	0.8507	1.108	0.9273	1.107	0.9197
0.968	0.8257	1.070	0.8937	0.969	0.8260	1.027	0.8738	1.151	0.9447	1.156	0.9409
1.015	0.8584	1.122	0.9223	1.000	0.8498	1.063	0.8962	1.194	0.9616	1.204	0.9577
1.063	0.8901	1.175	0.9474	1.031	0.8712	1.098	0.9154	1.237	0.9751	1.253	0.9724
1.110	0.9191	1.227	0.9641	1.063	0.8880	1.134	0.9335	1.280	0.9839	1.302	0.9828
1.158	0.9421	1.280	0.9785	1.094	0.9072	1.170	0.9489	1.323	0.9901	1.350	0.9895
1.205	0.9590	1.332	0.9874	1.126	0.9244	1.205	0.9624	1.366	0.9933	1.399	0.9931
1.253	0.9724	1.385	0.9926	1.157	0.9397	1.241	0.9731	1.409	0.9961	1.448	0.9952
1.300	0.9826	1.437	0.9962	1.189	0.9540	1.277	0.9815				
1.348	0.9896			1.220	0.9646	1.313	0.9875				
1.395	0.9936			1.252	0.9742	1.348	0.9915				
1.443	0.9962			1.283	0.9809	1.384	0.9942				
				1.315	0.9862	1.420	0.9958				
				1.346	0.9899						
				1.378	0.9929						
				1.409	0.9948						
				1.441	0.9962						

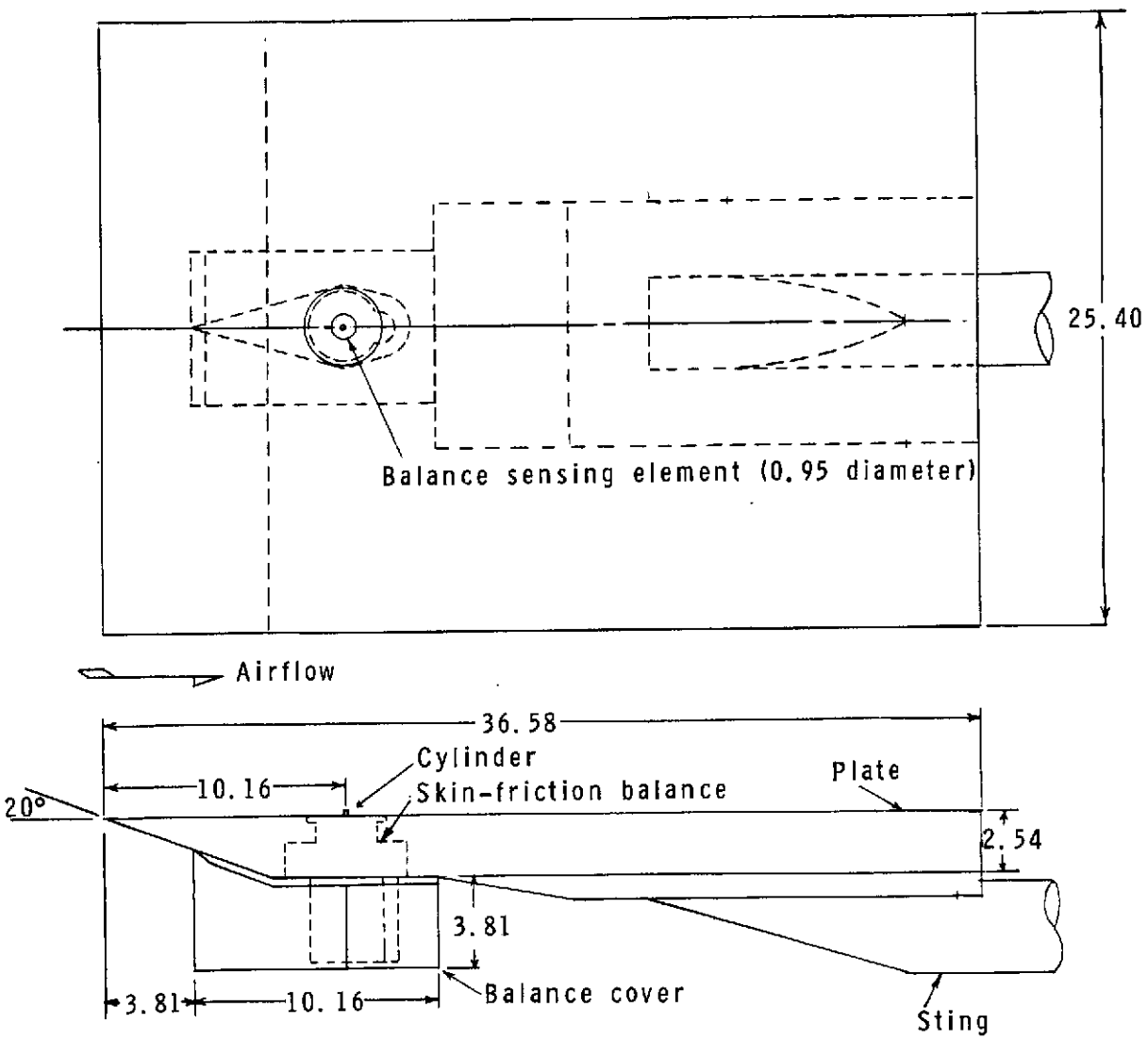

(a) Flat-plate model. (All dimensions are in centimeters.)

Figure 1.– Model and apparatus.

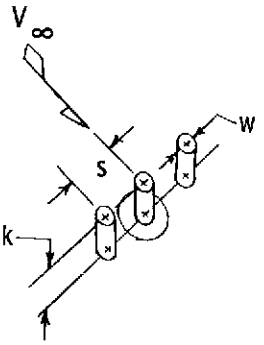

Cylinder configurations			
k, cm	w, cm	s/w	Number of cylinders
0.239	0.127	∞	1
		5	13
		10	9
		15	9
		20	9
.239	.239	∞	1
		3	13
		4	11
		6	11
		10	9
.127	.127	∞	1
		5	13
		10	9

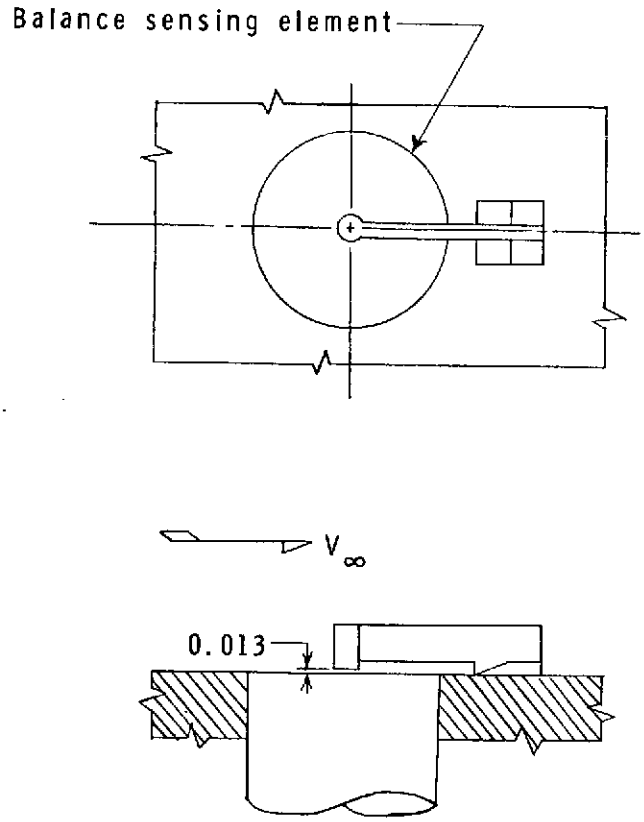

Cantilevered cylinder configuration

(b) Cylinder models.

Figure 1.- Continued.

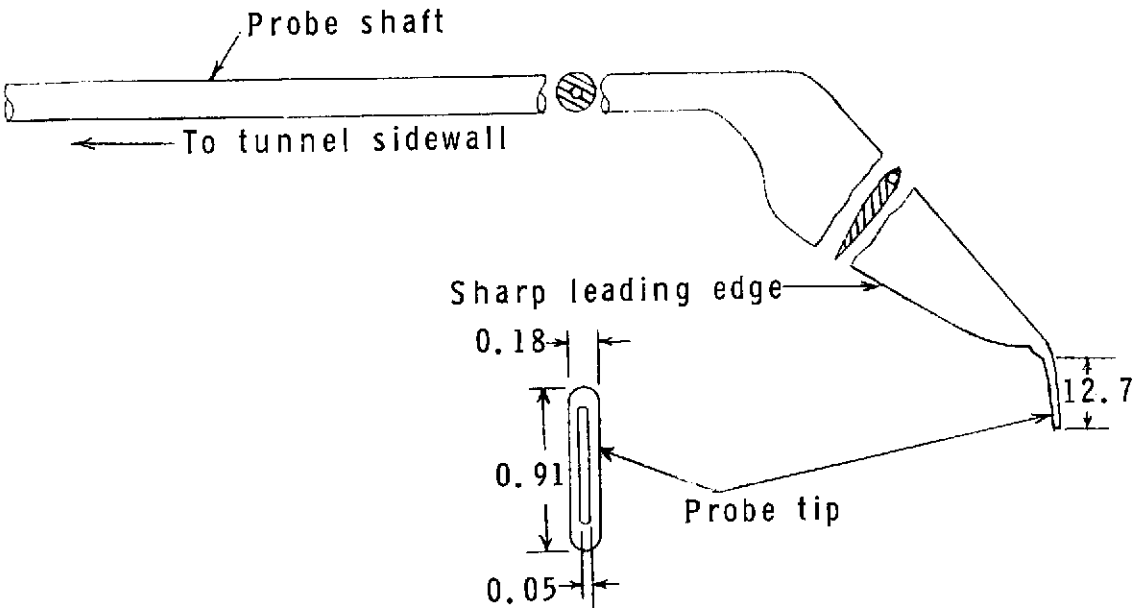

(c) Survey probe. (Dimensions are in millimeters.)

Figure 1.– Concluded.

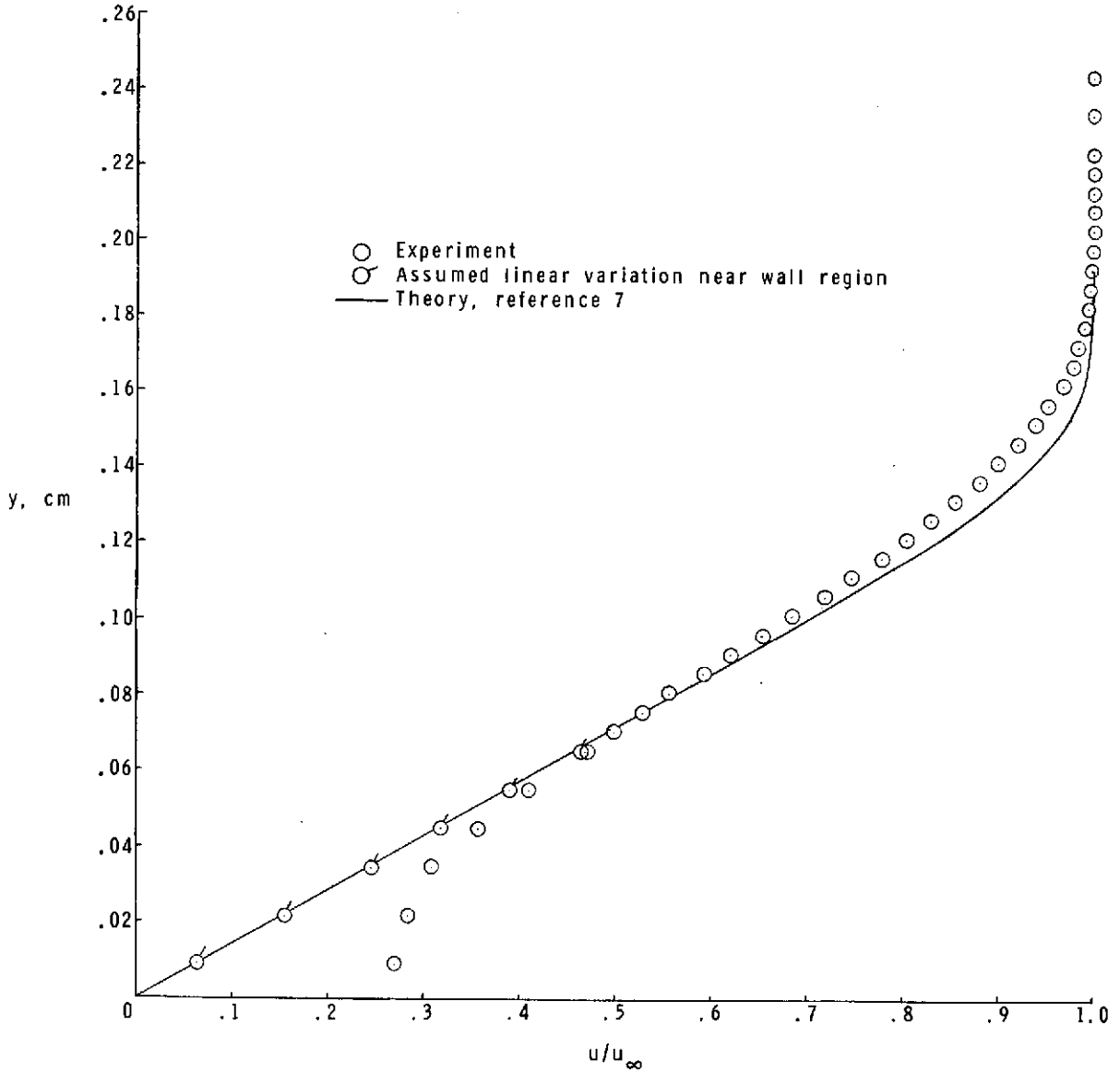

Figure 2.– Typical experimental velocity profile. $M_\infty = 3.95$; $R = 0.50 \times 10^6$.

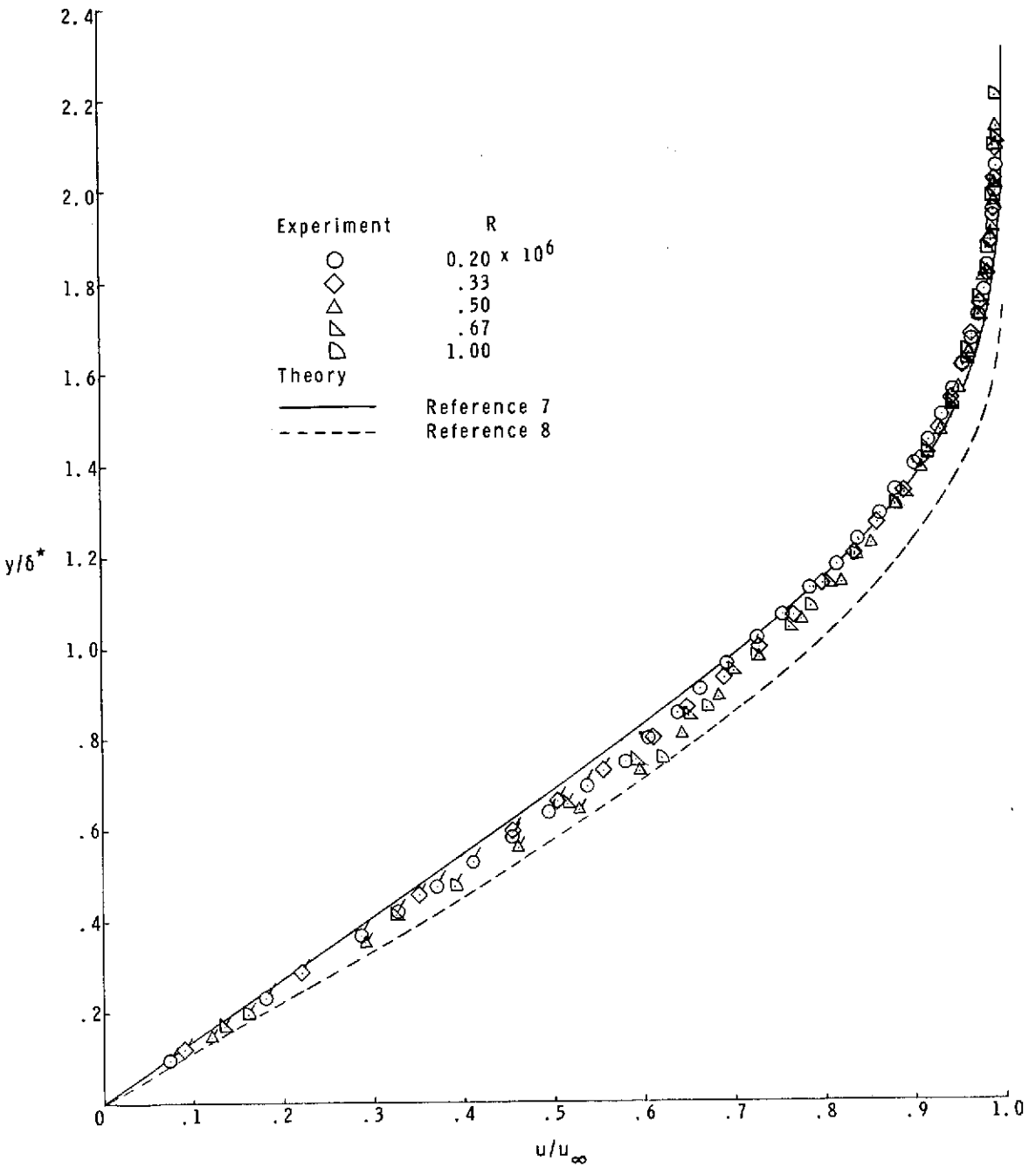

(a) $M_\infty = 2.30$.

Figure 3.– Comparison of experimental and theoretical velocity profiles. (Flagged symbols denote linear variation of u/u_∞ with y/δ^* assumed near wall region.)

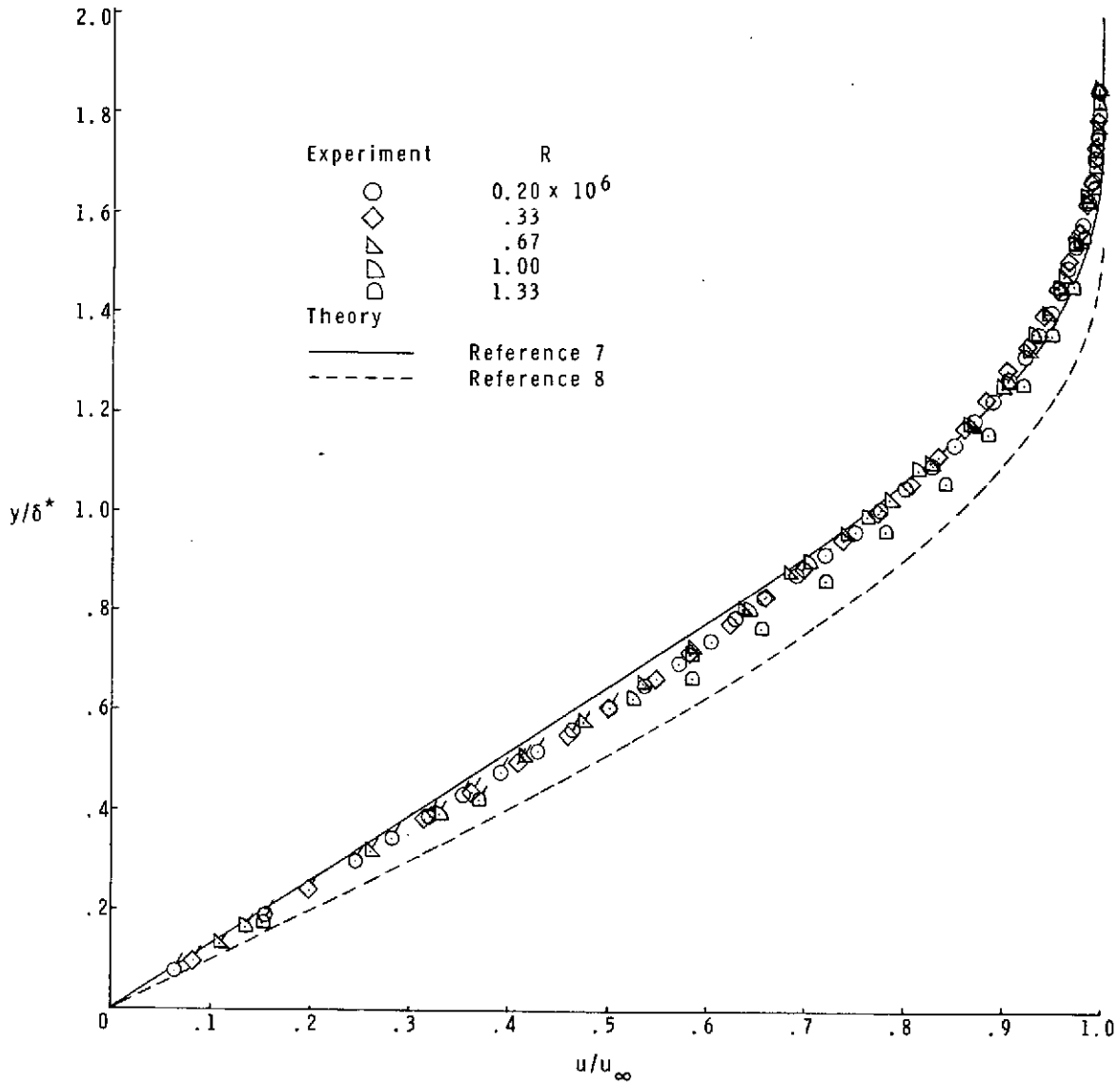

(b) $M_\infty = 2.90$.

Figure 3.– Continued.

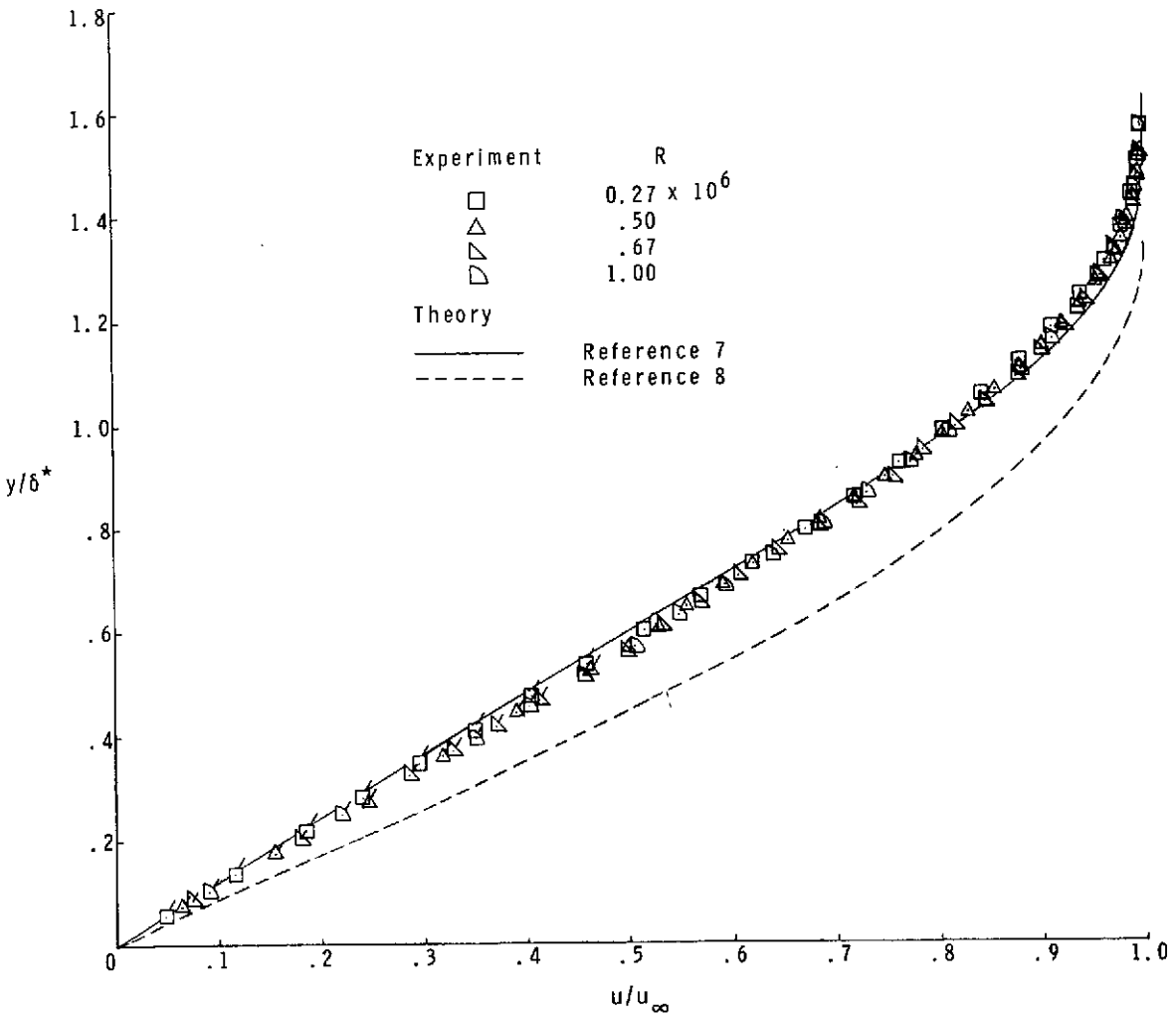

(c) $M_\infty = 3.95$.

Figure 3.– Continued.

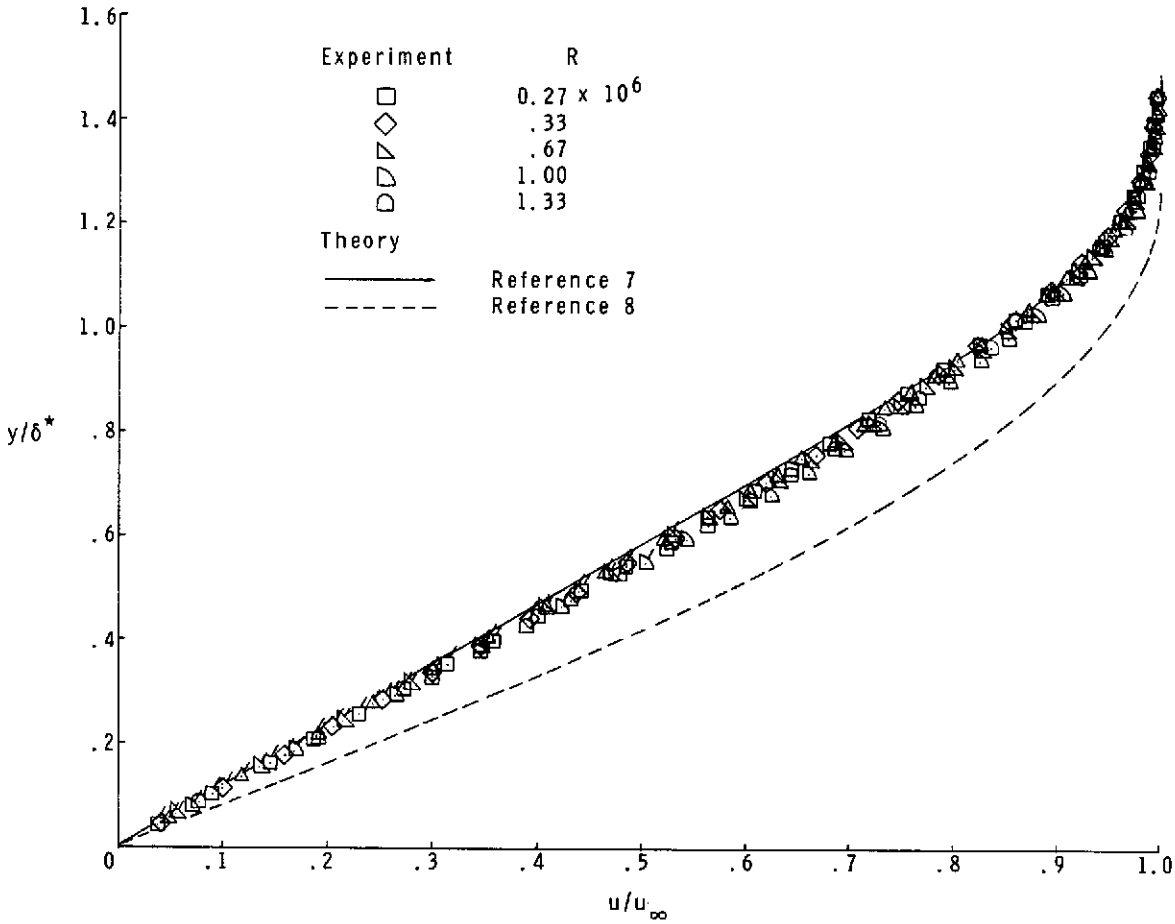

(d) $M_\infty = 4.60$.

Figure 3.– Concluded.

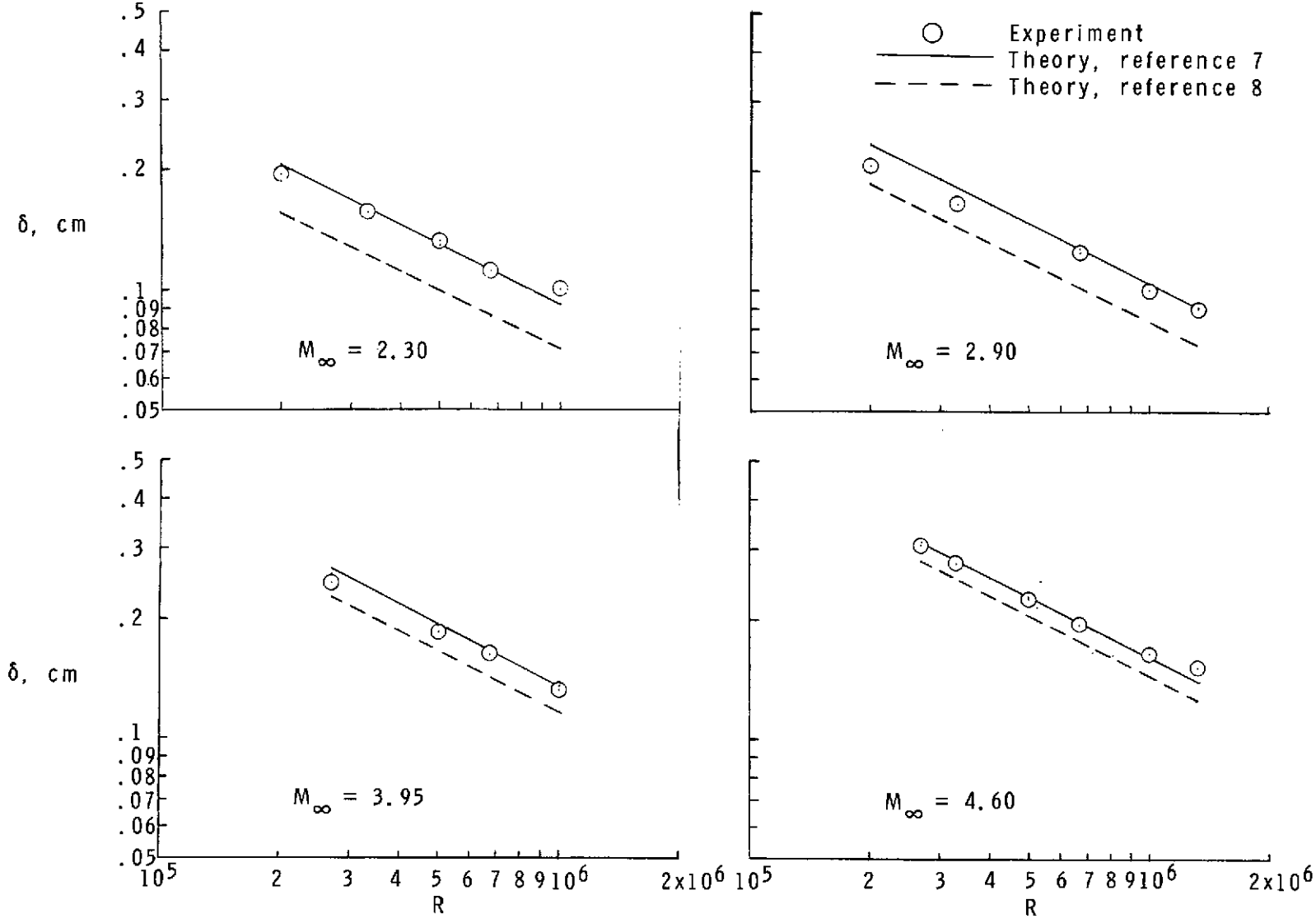

Figure 4.– Comparison of experimental and theoretical boundary-layer thicknesses.

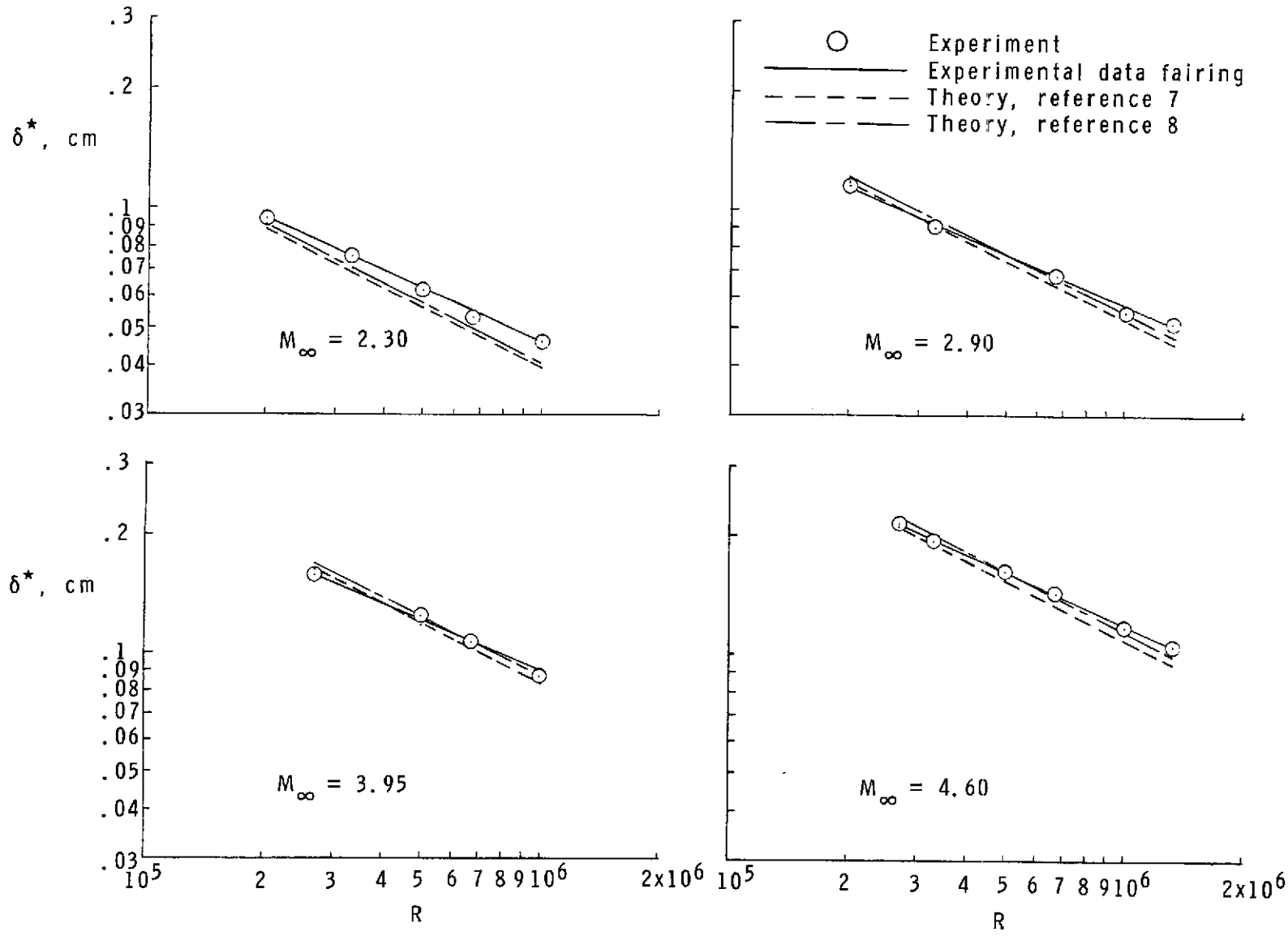

Figure 5.– Comparison of experimental and theoretical boundary-layer displacement thicknesses.

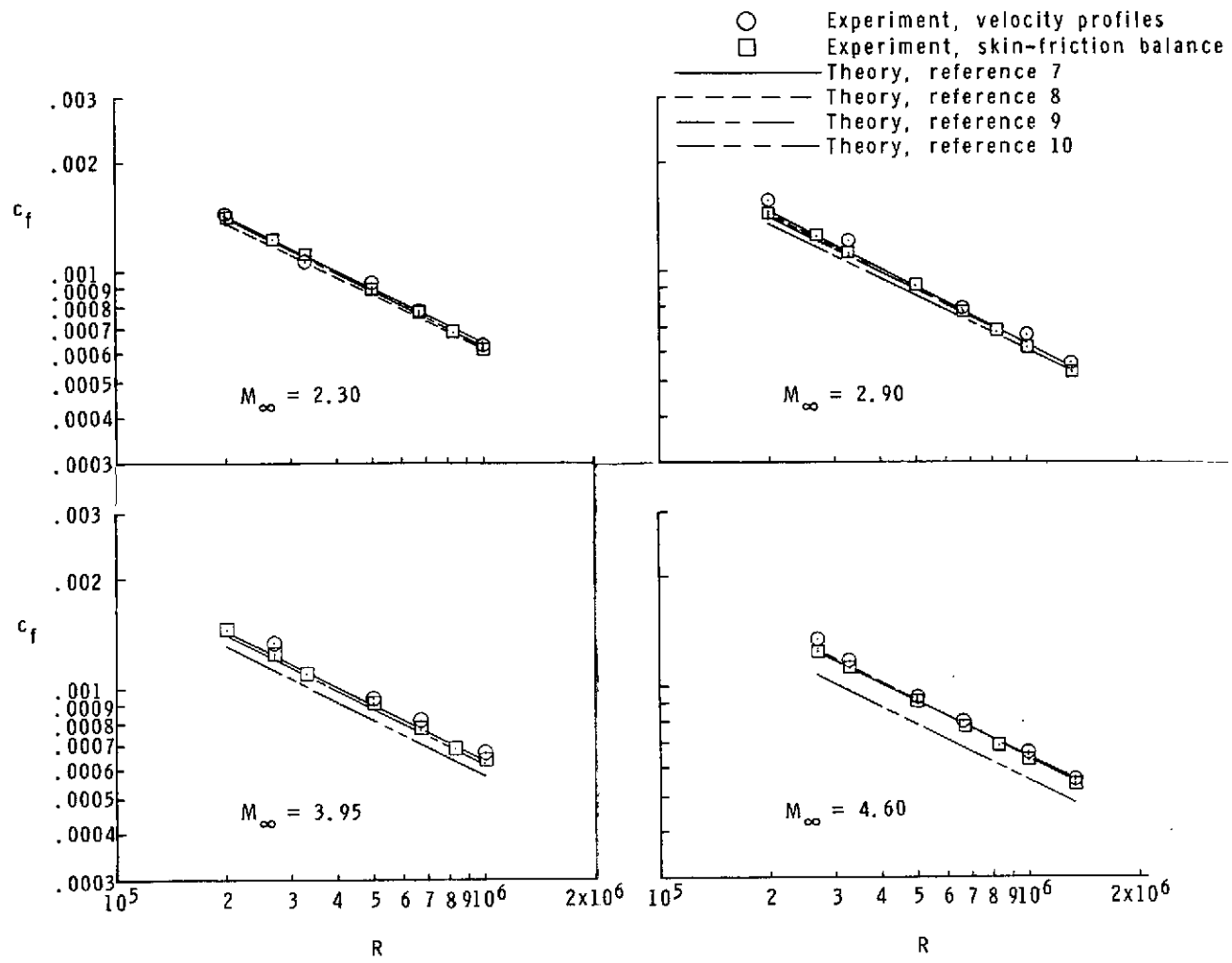

Figure 6.– Comparison of experimental and theoretical flat-plate skin-friction coefficients.

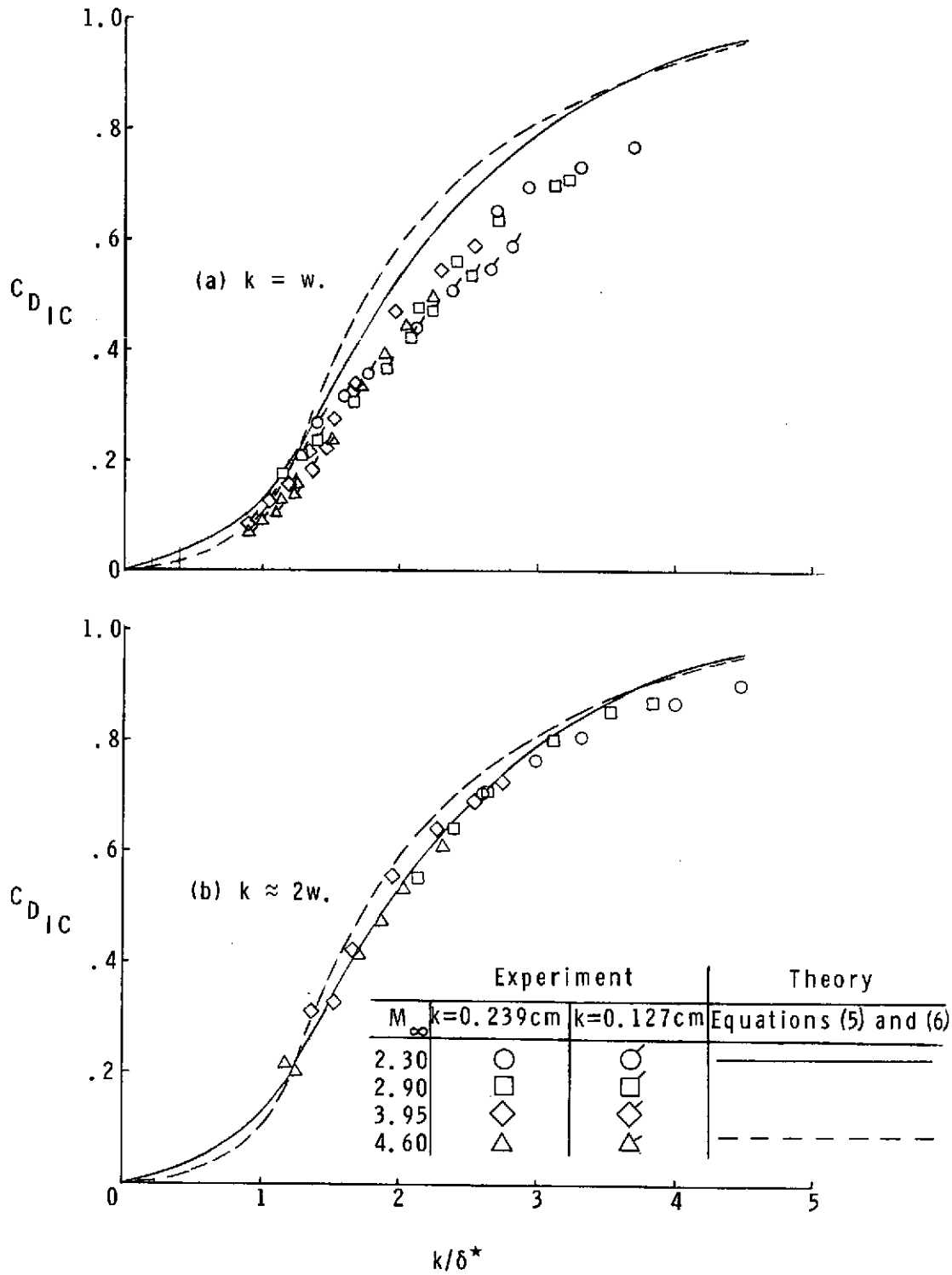

Figure 7.– Comparison of experimental and theoretical drag coefficients for isolated cylinders.

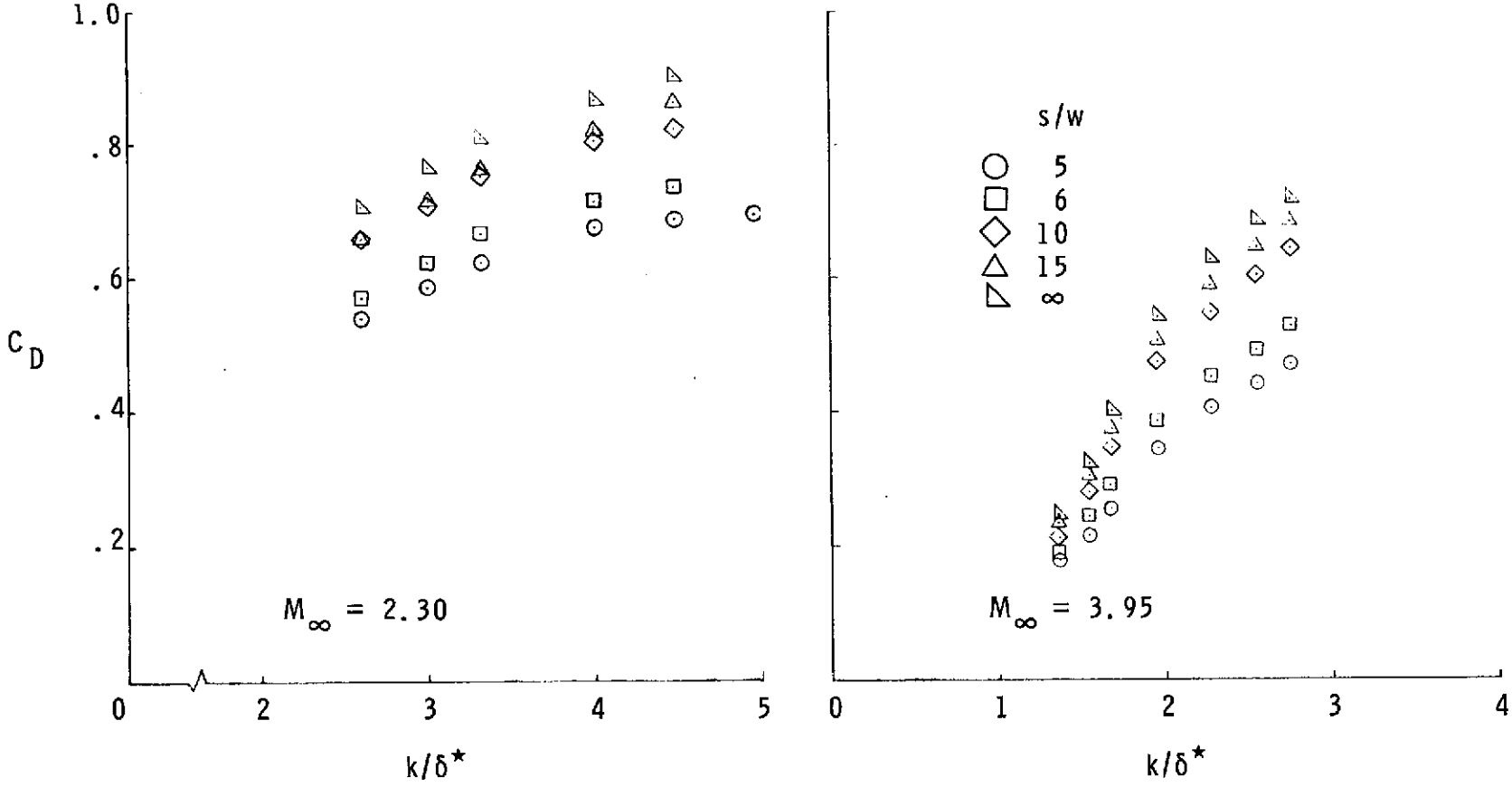

Figure 8.– Effect of spacing on cylinder drag. k = 0.239 cm ≈ 2w.

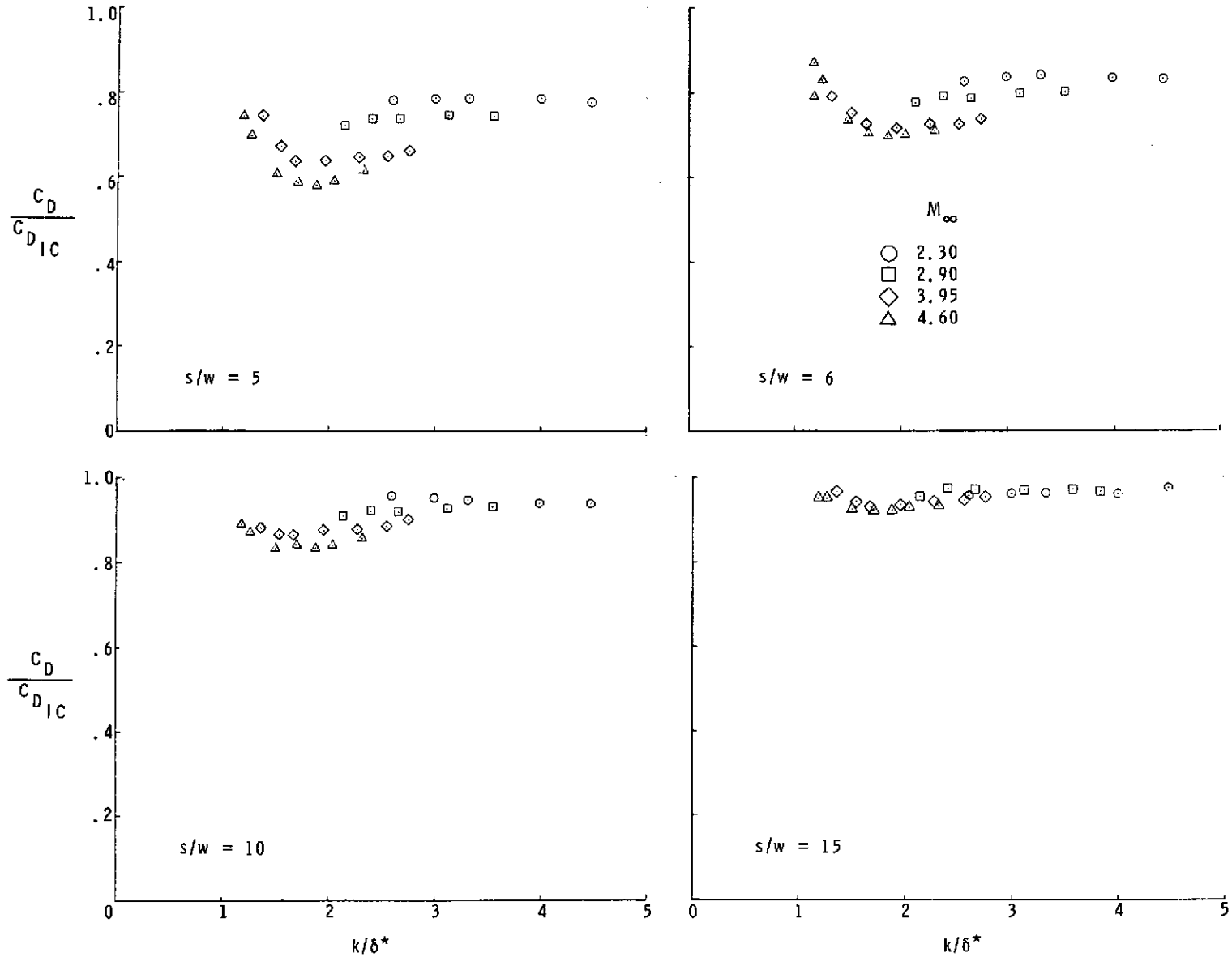

Figure 9.– Effect of cylinder spacing on normalized cylinder drag coefficients. k = 0.239 cm $\approx$ 2w.

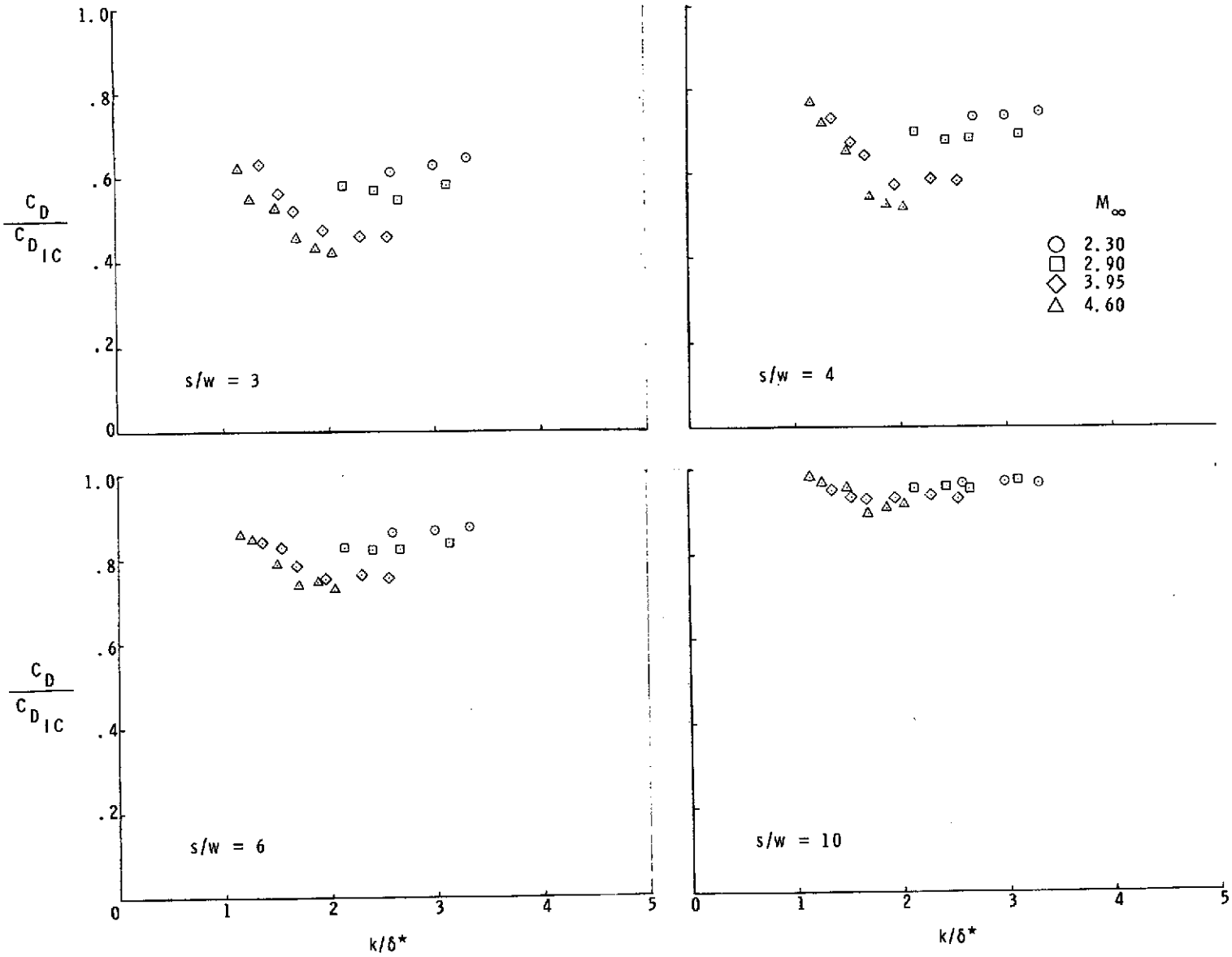

Figure 10.– Effect of cylinder spacing on normalized cylinder drag coefficients. k = 0.239 cm = w.

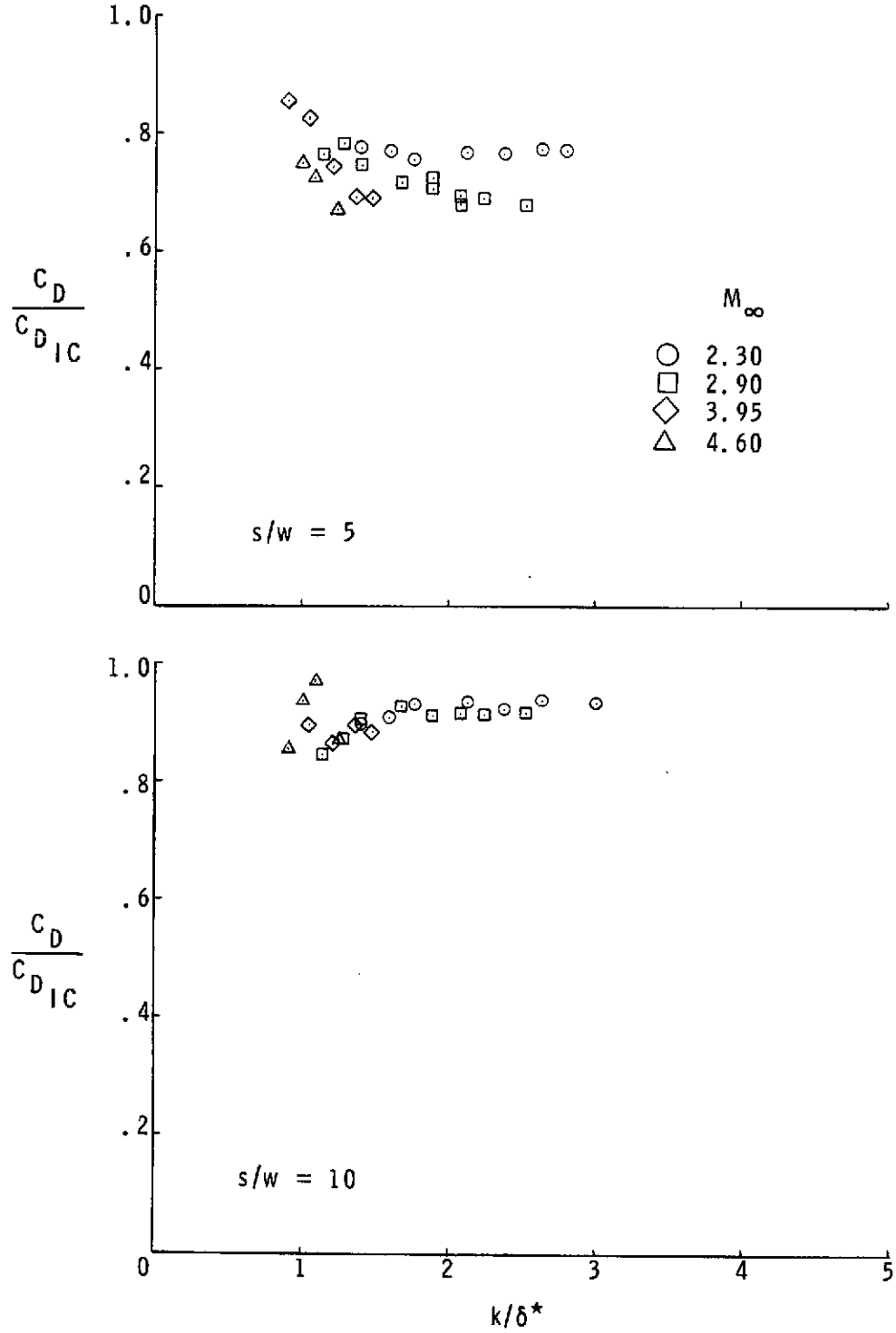

Figure 11.– Effect of cylinder spacing on normalized cylinder drag coefficients. k = 0.127 cm = w.

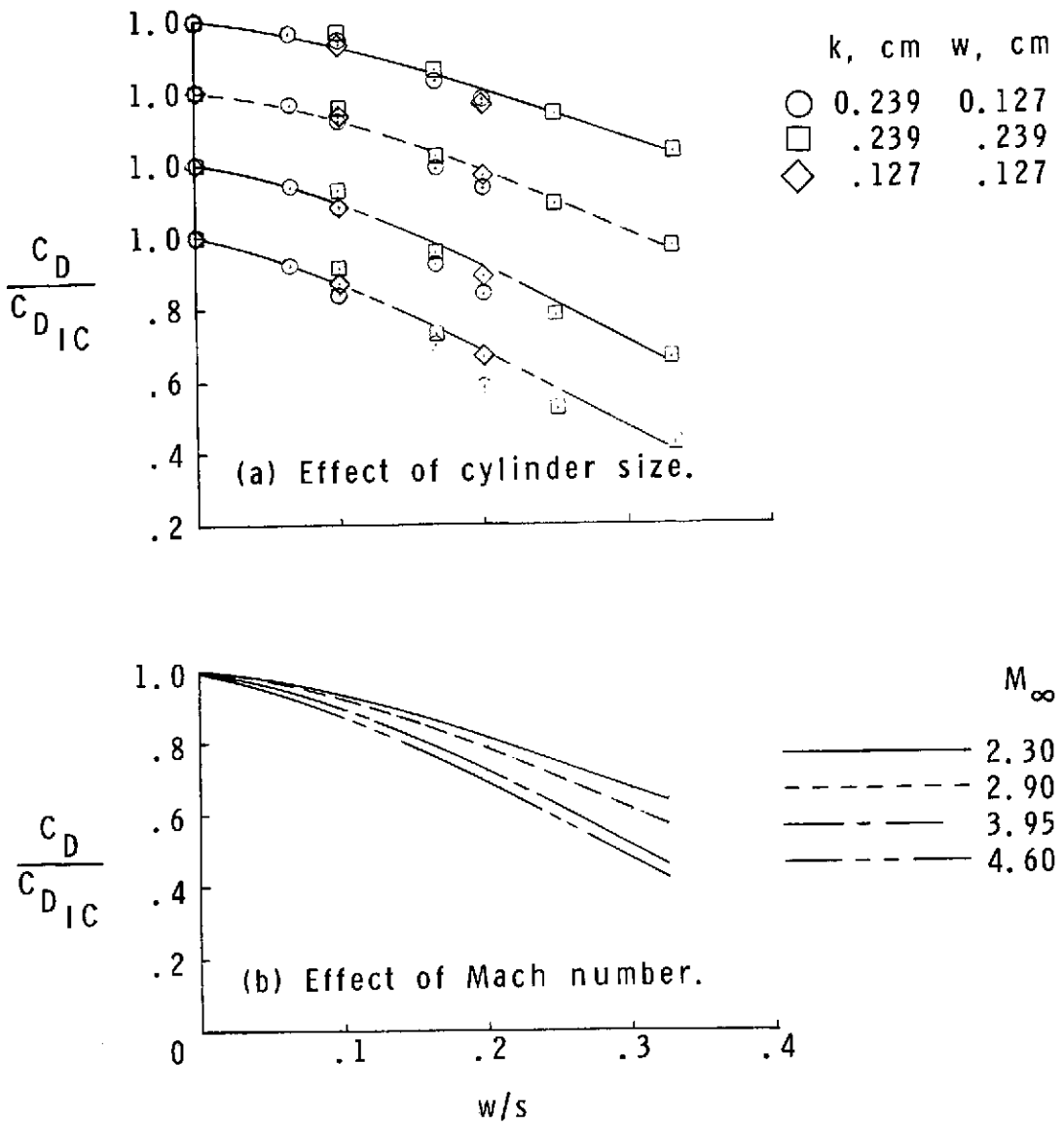

Figure 12.– Effect of cylinder size and Mach number on normalized drag coefficients. $k/\delta^* \gtrsim 2$.

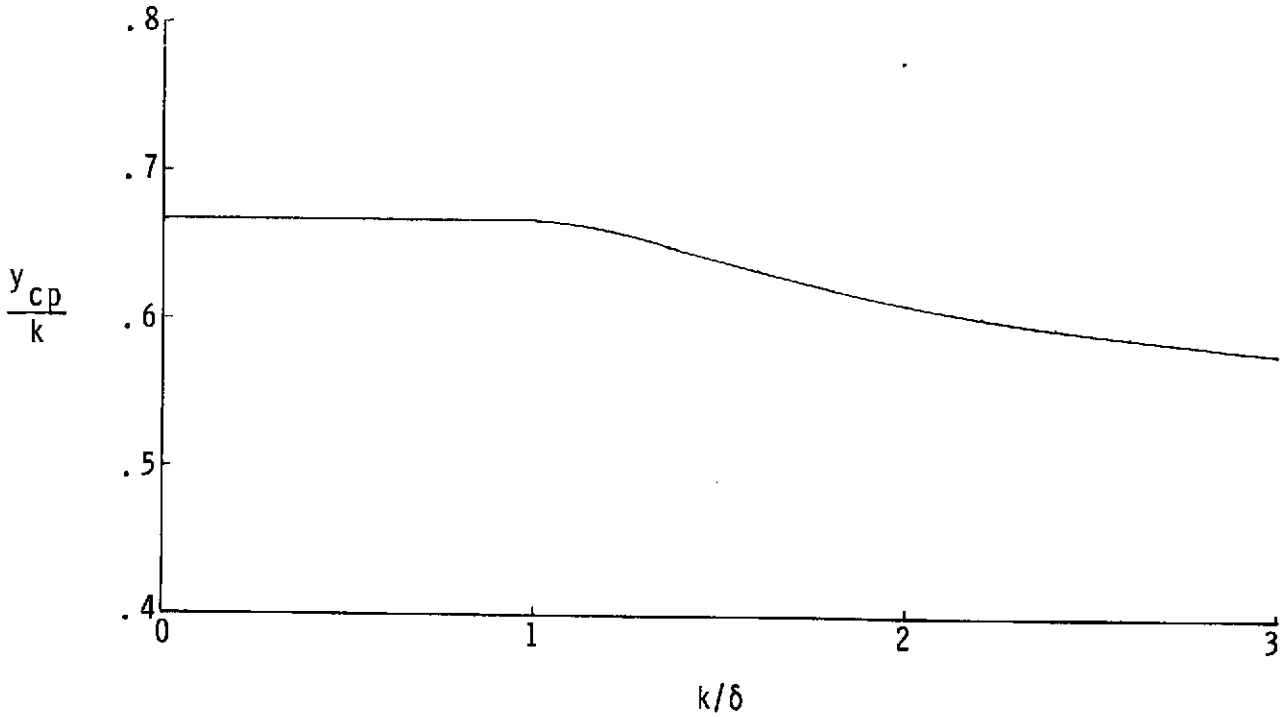

Figure 13.– Estimated center-of-pressure locations for cylinders. Equation (A12) for $\frac{k}{\delta} \geq 1$; equation (A13) for $\frac{k}{\delta} \leq 1$.

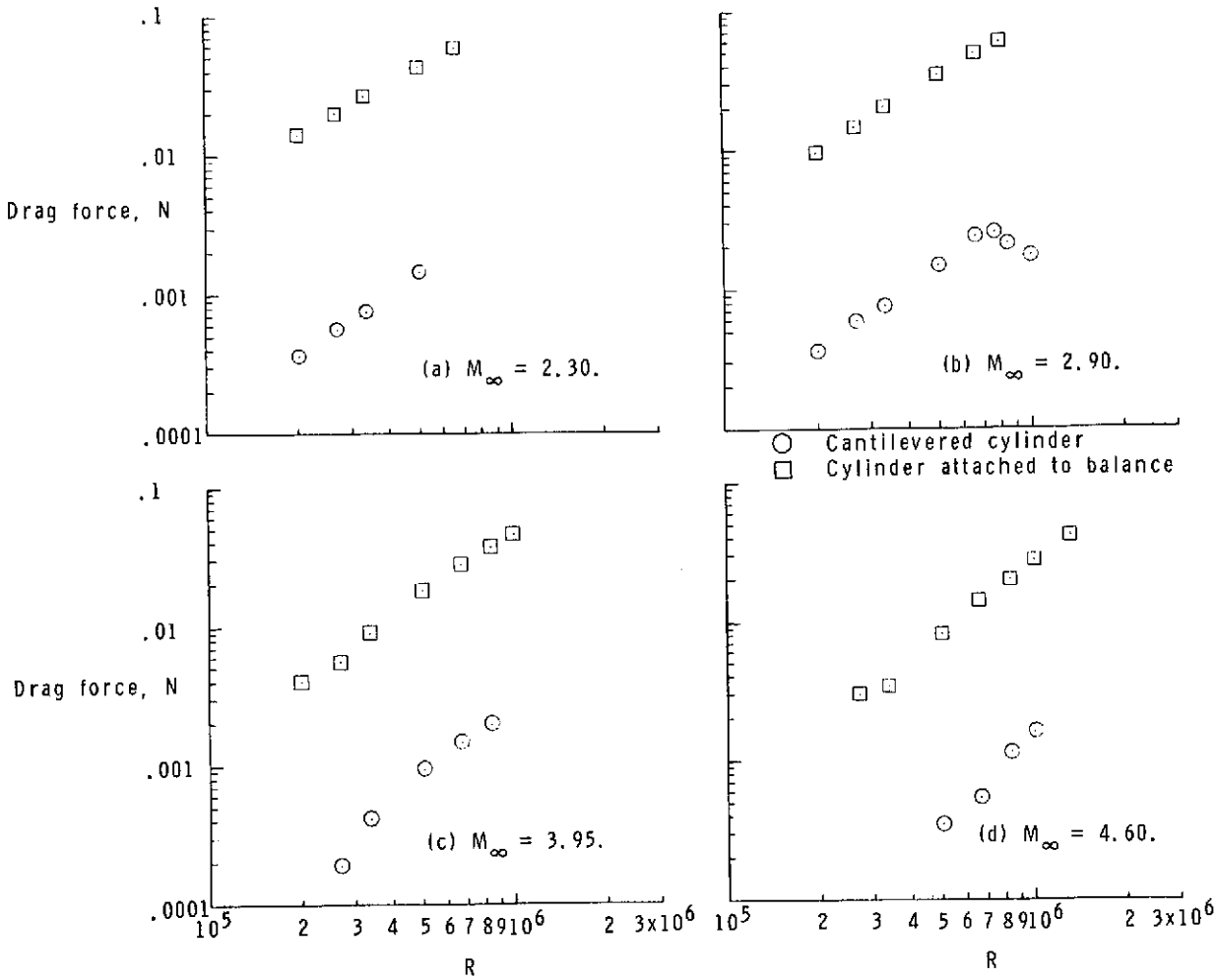

Figure 14.– Balance measurements using cantilevered cylinder installation and normal cylinder installation.